

AIVP

ADVANCES IN IMAGE AND VIDEO PROCESSING



TABLE OF CONTENTS

EDITORIAL ADVISORY BOARD	I
DISCLAIMER	II
Robust Watermarking for Color Images using SVD With Column/Row Wavelet Transforms in Low and Mid-Frequency Spectrum of Host H. B. Kekre, Tanuja Sarode and Shachi Natu	1
New Hybrid Approach for Identification of Spermatozoa in Human Semen Sample using Microscope Image Processing Techniques Nandini M. Chaudhari and B. V. Pawar	15
Medical Image Compression using DCT and DWT Techniques Gullanar M. Hadi	25
Saving of Etalons in Image Processing Systems Based on the Parallel Shift Technology Stepan Bilan, Sergey Yuzhakov and Sergii Bilan	36

EDITORIAL ADVISORY BOARD

Dr Zezhi Chen

Faculty of Science, Engineering and Computing; Kingston University London
United Kingdom

Professor Don Liu

College of Engineering and Science, Louisiana Tech University, Ruston,
United States

Dr Lei Cao

Department of Electrical Engineering, University of Mississippi,
United States

Professor Simon X. Yang

Advanced Robotics & Intelligent Systems (ARIS) Laboratory, University of Guelph,
Canada

Dr Luis Rodolfo Garcia

College of Science and Engineering, Texas A&M University, Corpus Christi
United States

Dr Kyriakos G Vamvoudakis

Dept of Electrical and Computer Engineering, University of California Santa Barbara
United States

Professor Nicoladie Tam

University of North Texas, Denton, Texas
United States

Professor Shahram Latifi

Dept. of Electrical & Computer Engineering University of Nevada, Las Vegas
United States

Professor Hong Zhou

Department of Applied Mathematics Naval Postgraduate School Monterey, CA
United States

Dr Yuriy Polyakov

Computer Science Department, New Jersey Institute of Technology, Newark
United States

Dr M. M. Faraz

Faculty of Science Engineering and Computing, Kingston University London
United Kingdom

DISCLAIMER

All the contributions are published in good faith and intentions to promote and encourage research activities around the globe. The contributions are property of their respective authors/owners and the journal is not responsible for any content that hurts someone's views or feelings etc.

Robust Watermarking for Color Images using SVD with Column/Row Wavelet Transforms in Low and Mid-Frequency Spectrum of Host

H. B. Kekre¹, Tanuja Sarode² and Shachi Natu³

¹MPSTME, NMIMS University Mumbai, India

²TSEC, Mumbai University, Mumbai,

³NMIMS University, Mumbai;

¹hbkekcre@yahoo.com, ²tanuja_0123@yahoo.com, ³shachi_natu@yahoo.com

ABSTRACT

This paper proposes a joint SVD and wavelet transform based watermarking technique. Host and watermark images are column/row transformed using wavelet transforms like DCT wavelet, Walsh wavelet, Haar wavelet and DKT wavelet. These wavelet transforms are generated from orthogonal transforms DCT, Walsh, Haar and DKT. Generally middle frequency region of transformed host is used to hide the watermark. However, in proposed technique, stability of SVD is exploited to hide the watermark in low frequency region of host. Singular values of low as well as middle frequency region of transformed host are altered with suitable scaling factors to hide the watermark. Performance of the technique is tested under compression, cropping, noise addition and resizing attack. Use of low frequency region in proposed method shows strong robustness for all attacks except cropping and is immediately followed by use of mid-frequency region. To sustain against cropping attack, mid-frequency region is found to be more suitable.

Keywords: Watermarking, Singular Value Decomposition, column wavelet transform, row wavelet transform, Discrete Kekre Transform (DKT), Binary distributed run length noise, Gaussian Distributed run length noise, JPEG compression.

1 Introduction

Watermarking is the process of hiding some information in multimedia contents such as image, audio or video file to protect it from copyright abuse [1]. Two major constraints that need to be followed while watermarking the digital contents are robustness and visual imperceptibility of hidden information. In recent years, use of transforms is gaining popularity in the process of watermarking as it is more robust than spatial domain watermarking techniques. DCT, DFT, wavelet transform prove to be more robust in digital watermarking process. Combining two or more transforms together has also become quite popular to increase the robustness. Singular Value decomposition (SVD) and Discrete Wavelet Transform (DWT) [2, 3, 4, 5], DCT-DWT [6, 7, 8], DCT_DWT_SVD [9, 10] are the commonly used combinations of transforms in watermarking. In this paper a hybrid watermarking technique using SVD and column/row wavelet transform generated from orthogonal transforms DCT, Walsh, Haar and Discrete Kekre Transform is proposed. Middle frequency band and low frequency band of column/row wavelet transformed image is used to embed the singular values of watermark. Proposed method is evaluated against compression, cropping, noise addition, and image resizing. Remaining paper is organized as follows: section 2

discusses existing work in digital image watermarking field. Section 3 explains singular value decomposition and wavelet transforms. Section 4 explains proposed method. Section 5 evaluates the performance of proposed technique against various attacks. Section 6 ends the paper with conclusion.

2 Related Work

Qiang Li, Chun Yuan, Yu-Zhuo Zhong proposed a hybrid DWT-SVD based watermarking considering human visual properties [2]. Host image is divided into four sub bands and each band is subjected to SVD. Singular values of watermark are embedded in these singular values of host. The embedding strength is determined by a human visual model proposed in A.S. Lewis and G. Knowles, (1992) and improved in M. Bertran et al., (2001). The scheme is claimed to be robust for its embedding data into all frequencies and large capacity for using SVD. In addition, the use of human visual model guarantees the imperceptibility of the watermark.

In [11] a robust hybrid image watermarking scheme based on SVD and DCT is proposed. After applying SVD to the cover image blocks, DCT on the macro block comprised of the first singular values of each image block is applied. Watermark is embedded in the high-frequency band of the SVD-DCT block by imposing a particular relationship between some pseudo-randomly selected pairs of the DCT coefficients. In [12] a method of non-blind transform domain watermarking based on DWT-DCT-SVD is proposed. The DCT coefficients of the DWT coefficients are used to embed the watermarking information. This method of watermarking is found to be robust and the visual watermark is recoverable without any perceivable amount of distortion even in the case of attacks. In [13] authors proposed implementation and performance analysis of two different watermarking schemes based on DCT-DWT-SVD. One is based on SVD of DC coefficients using second level DWT decomposition and other is considering SVD of all DCT values of second level DWT composition of cover image. Effectiveness of proposed schemes is measured using PSNR and Normalized Cross Correlation (NCC).

A new SVD based and DCT-DWT oriented watermarking scheme is proposed in [9]. To achieve robustness with high perceptual transparency and low insertion ratio, the middle band DCT coefficients are chosen to achieve high robustness against JPEG compression. Robustness against other attacks is achieved by taking DWT of the DCT coefficients and the lowest frequency LL band of DWT is chosen for insertion. Insertion method in proposed technique uses SVD because slight variation of singular values does not change the visual perception of the image. To attain robustness and imperceptibility, a hybrid image-watermarking scheme based on Discrete Wavelet Transform (DWT) and Singular value decomposition (SVD) is proposed in [14]. The LH Band of the third level of image in DWT domain is modified with SVD to embed the singular value of watermark. The proposed embedding and extracting methodology was employed to accelerate the hybrid DWT-SVD watermarking and to avoid the leak of watermark. This hybrid technique results to optimize both (robustness and imperceptibility) the fundamentally conflicting requirements. Lagzian, Soryani and Fathy [15] proposed a watermarking scheme based on redundant discrete wavelet transform (RDWT) and Singular Value Decomposition (SVD). After applying RDWT to cover image, SVD is applied to each sub band. Then singular values of the cover image are modified using singular values of the visual watermark. The advantage of the proposed technique is its robustness against most common attacks in comparison to the DWT-SVD method.

In [16] a novel approach of watermarking for copyright protection applications using the singular value decomposition (SVD) in the dual tree complex wavelet transform (DT-CWT) domain is introduced. After applying the 2-level DT-CWT to the cover grayscale image, SVD of each high-pass sub band is obtained. These singular values are then modified by the singular values of the DT-CWT-transformed visual watermark. Modification in all sub bands allows the development of a watermarking scheme that is robust to a wide range of attacks. Wang et. al in [17] proposed a novel watermarking scheme for image authentication based on discrete wavelet transform (DWT) and singular value decomposition (SVD). Different from the developed SVD-based watermarking schemes where the singular values are slightly modified, this scheme constructs the watermarks from the singular vectors which specify intrinsic geometry properties of images. Within the framework of zero watermarking, the watermarks are registered in a third-part intellectual property rights (IPR) database for copyright protection. Experimental results show that this scheme is robust not only to common image processing operations, but also robust to local geometric distortions. A blind watermarking scheme based on the discrete wavelet transform (DWT) and singular value decomposition is proposed in [18]. Singular values of high frequency (HH) band are used to optimize perceptual transparency and robustness constraints. A joint DWT and DCT based watermarking technique with low frequency watermarking with weighted correction is proposed in [19]. DWT has excellent spatial localization, frequency spread and multi-resolution characteristics, which are similar to the theoretical models of the human visual system (HVS). DCT based watermarking techniques offer compression while DWT based watermarking techniques offer scalability. These desirable properties are used in this combined watermarking technique.

3 Wavelet Transforms and Singular Value Decomposition

Wavelets are mathematical functions that cut up data into different frequency components, and then study each component with a resolution matched to its scale [23]. Principal advantage of wavelet is that they provide time-frequency localization. Temporal analysis is performed with a contracted, high-frequency version of the prototype wavelet, while frequency analysis is performed with a dilated, low-frequency version of the same wavelet [23]. Wavelet transform used in the proposed method is generated using wavelet generation algorithm given in [23].

Using singular value decomposition, any real matrix A can be decomposed into a product of three matrices U , S and V as $A=USVT$, where U and V are orthogonal matrices and S is diagonal matrix. If A is $m \times n$ matrix, U is $m \times m$ orthonormal matrix whose columns are called as left singular vectors of A and V is $n \times n$ orthonormal matrix whose columns are called right singular vectors of A . For $m > n$, S takes the following form [20]:

$$S = \begin{bmatrix} s_1 & 0 & \dots & 0 \\ 0 & s_2 & \dots & 0 \\ \vdots & \vdots & \ddots & \vdots \\ 0 & \vdots & 0 & s_n \\ 0 & 0 & \dots & 0 \end{bmatrix}$$

The diagonal elements are listed in descending order, $s_1 \geq s_2 \geq \dots \geq s_n \geq 0$.

Some properties of SVD which make it useful in image processing are:

- The singular values are unique for a given matrix.
- The rank of matrix A is equal to its nonzero singular values. In many applications, the singular values of a matrix decrease quickly with increasing rank. This property allows us to reduce the noise or compress the matrix data by eliminating the small singular values or the higher ranks [21].

- The singular values of an image have very good stability i.e. when a small perturbation is added to an image; its singular values don't change significantly [22].

4 Proposed Method

In the proposed method, DCT wavelet, Walsh wavelet, Haar wavelet and DKT wavelet transforms are used generated from orthogonal transforms DCT, Walsh, Haar and DKT respectively by using the algorithm in [23]. Since, different size combinations are possible to generate desired size wavelet transform matrix, all such possible size combinations are tried and the best size combination is selected for experimental work. For watermark image, (32, and 4) and for host image (16, 16) pair of component orthogonal transforms is observed to give best robustness and hence it is selected. A test set of five color bitmap host images (256x256) and a watermark (128x128) is used.



Figure 1 (a)-(e) Host images and (f) watermark image used for experimental work

Embedding and extraction procedures explained below are followed on each plane of host and watermark image separately.

4.1 Steps for embedding

- Step 1.** Apply column/row wavelet transform to host and watermark image.
- Step 2.** Perform Singular value decomposition on column/row transformed watermark image. Since watermark is of size 128x128, it gives 128 singular values.
- Step 3.** Due to high energy compaction property of SVD, only few of these singular values hold maximum energy of image and are sufficient for embedding in host. In proposed experimental work it has been observed that only first 30 singular values pack almost 99% of image energy and hence are selected for embedding.
- Step 4.** To embed 30 singular values in host, frequency band of 30 rows/columns is selected from column/rows transformed host image. After testing various middle frequency rows/columns for robustness it is observed that frequency band ranging from row/column 101 to 130 is better than other rows/columns. Also a low frequency band of rows/columns 1 to 30 is selected for embedding the watermark.
- Step 5.** Singular value decomposition of selected low / mid frequency band of host is obtained. These singular values of host are now replaced by singular values of column/row transformed watermark. Each singular value of watermark is adaptively scaled down to match with the singular value of host frequency band in order to minimize the distortion in watermarked image. These scaling factors are preserved for use in extraction process.
- Step 6.** Inverse SVD followed by inverse column/row transform is obtained to get watermarked image. Imperceptibility of proposed technique is measured by calculating average of absolute pixel difference (Mean Absolute Error) between host and watermarked image.

Watermarked image obtained through embedding process is tested under various image processing attacks and from these attacked watermarked images; watermark is extracted using extraction procedure as described below.

4.2 Extraction procedure

Extraction procedure is performed on watermarked image in the following manner:

- Step 1.** Take column/row wavelet transform of watermarked/attacked watermarked image. Select the frequency band (low / middle) in which embedding is done.
- Step 2.** Perform SVD on this frequency band and scale up the obtained singular values using adaptive scaling factors preserved in embedding process.
- Step 3.** Perform inverse singular value decomposition using these singular values to get the extracted watermark.
- Step 4.** Robustness of proposed technique is measured using Average absolute pixel difference (MAE) between embedded and extracted watermark.

5 Performance Analysis of Proposed Technique against Various Attacks

Watermarked images are subjected to attacks like compression, cropping, noise addition, resizing. Performance of each of these attacks when watermark is embedded in low frequency band and middle frequency band is evaluated.

5.1 Compression attack

Watermarked images are subjected to compression using different techniques namely compression using transforms, compression using Vector Quantization and JPEG compression.

DCT, DST, Walsh, Haar and DCT wavelet are the transforms used for transform based compression. In VQ based compression KFCG [24] algorithm is used and a codebook of size 256 is generated to compress the image. In JPEG compression, 100% quality factor is used to compress the image.

Watermarked images after performing compression attack using Haar and watermark extracted from it are shown in Figure 2. These images are for embedding done in low and middle frequency bands. For each of these images, MAE is given below it.


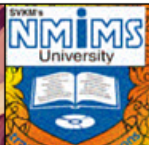





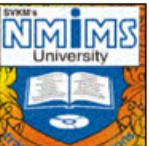
							
(a) DCT column wavelet transform rows 1-30		(b) DCT column wavelet transform rows 101-130		(c) DCT row wavelet transform columns 1-30		(d) DCT row wavelet transform columns 101-130	

Figure 2 watermarked images after performing compression attack using Haar and watermark extracted from them (a) when watermark is embedded in low frequency band of DCT column wavelet transform (b) when watermark is embedded in middle frequency band of DCT column wavelet transform (c) when watermark is embedded in low frequency band of DCT row wavelet transform (d) when watermark is embedded in middle frequency band of DCT row wavelet transform.

Summary of different types of compression attacks is given in Figure 3 to Figure 6. Figure 3 shows performance of various column wavelet transforms against compression using DCT, DST, Walsh and Haar when watermark is embedded in low frequency region (rows/columns 1 to 30) and middle frequency region (rows/columns 101 to 130).

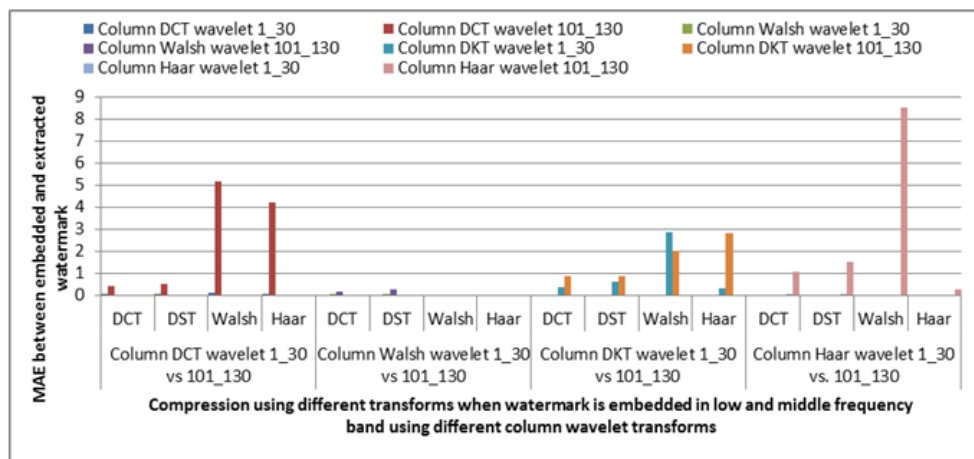


Figure 3 Comparison of MAE between embedded and extracted watermark against compression using DCT, DST, Walsh and Haar when watermark is embedded in low and middle frequency elements using different column wavelet transforms.

From Figure 3, it is observed that all column transforms used for watermark embedding give excellent robustness against compression attack using DCT and DST when watermark is embedded in low or middle frequency band. Column DCT wavelet and column Haar wavelet show little increase in MAE when compression is performed using Walsh and embedding is done in middle frequency region. However this increase is not spoiling the quality of recovered watermark and still can be considered as very good performance against compression attack. Thus proposed method is highly robust for almost all transform based compression attacks.

Figure 4 compares performance of each column wavelet transforms against compression using DCT wavelet, JPEG compression and VQ based compression when watermark is inserted in low and middle frequency elements.

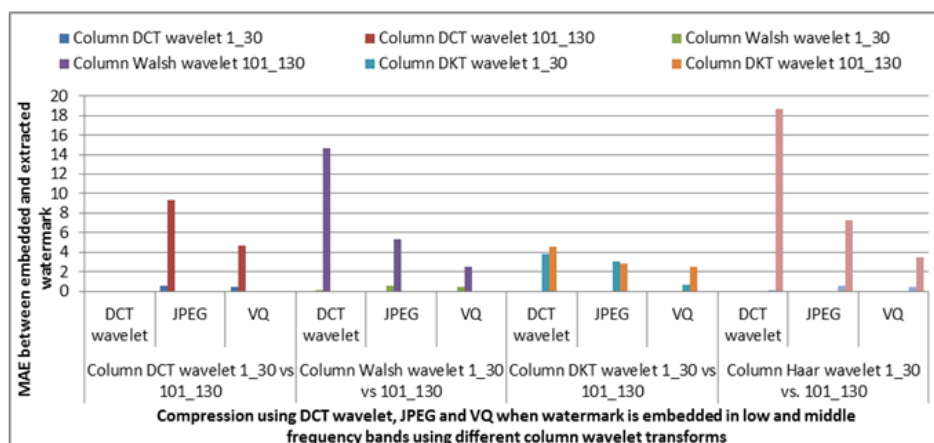


Figure 4 Comparison of MAE between embedded and extracted watermark against compression using DCT wavelet, JPEG compression and Vector Quantization when watermark is embedded in low and middle frequency elements using different column wavelet transforms.

In low frequency region, all column wavelet transforms exhibit very good robustness against compression using DCT wavelet, JPEG compression and VQ based compression. When embedding is done in middle frequency region, column Walsh wavelet and column Haar wavelet performance against DCT wavelet based compression is slightly degraded. For JPEG and VQ based compression all column wavelet transforms exhibit high sustainability.

Figure 5 shows performance comparison against compression using different transforms when embedding in low and middle frequency is done using row wavelet transforms.

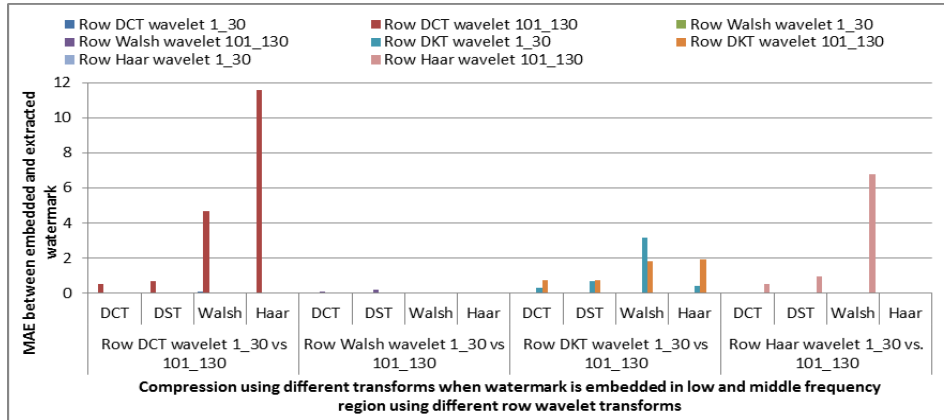


Figure 5 Comparison of MAE between embedded and extracted watermark against compression using DCT, DST, Walsh and Haar when watermark is embedded in low and middle frequency elements using different row wavelet transforms

Similar to column wavelet transform behavior, row DCT wavelet shows excellent robustness against compression when low frequency region is used for embedding. For middle frequency region embedding, DCT wavelet shows very good robustness for DCT and DST and Walsh compression. For Haar based compression, row DCT wavelet performance is poorer as compared to Walsh wavelet, Haar wavelet and DKT wavelet. Row Walsh wavelet transform also shows good sustenance for all transform based attacks when watermark is embedded in middle frequency as well as low frequency singular values. Row DKT wavelet is also observed to be robust for all transform based compression attacks when watermark is embedded in low and middle frequency band singular values. Row Haar wavelet transform shows excellent robustness for DCT, DST and Haar based compression irrespective of frequency band used for embedding. For Walsh based compression it shows higher MAE when embedding is done in middle frequency region. In all Row wavelet transforms also show very good robustness against compression using DCT, DST, Walsh and Haar when watermark is embedded in singular values of low frequency region.

Figure 6 compares performance of embedding in low and middle frequency regions using different row wavelet transforms against compression using DCT wavelet, JPEG compression and VQ based compression.

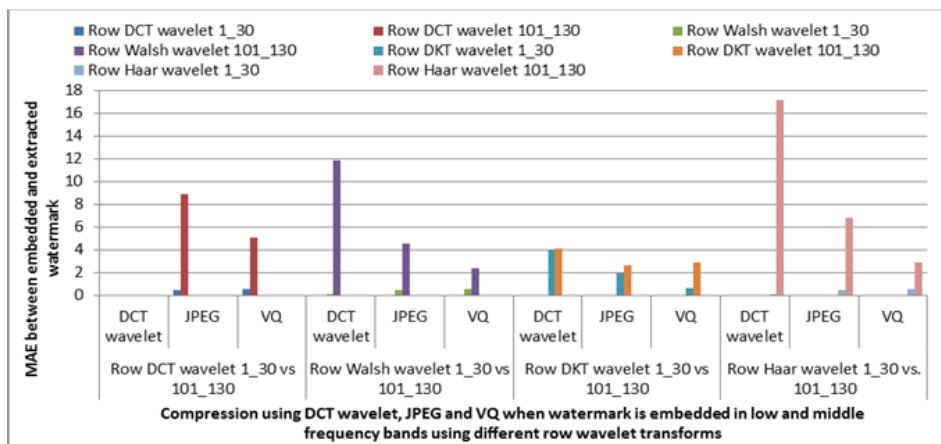


Figure 6 Comparison of MAE between embedded and extracted watermark against compression using DCT wavelet, JPEG compression and Vector Quantization when watermark is embedded in low and middle frequency elements using different row wavelet transforms

From Figure 6, we can see that for compression using DCT wavelet, embedding watermark in low frequency region, all row wavelet transform used for embedding, shows excellent sustenance. Row DCT wavelet and row DKT wavelet also sustain this attack when watermark is embedded in middle frequency region. However, row Walsh wavelet and row Haar wavelet show poor resistance against DCT wavelet based compression when embedding is performed in middle frequency region. For JPEG and VQ based compression though use of low frequency band shows better sustenance than middle frequency region, both regions can be concluded to show excellent robustness.

5.2 Cropping of watermarked images

Different amount of information is cropped from watermarked images by cutting the 16x16 size square portion at corners, 32x32 size square portions at corners and 32x32 size square portions at the center of watermarked image. Figure 7 shows result images for cropping 32x32 at center and using DCT column wavelet for embedding watermark. Sustenance of proposed method against such cropping when singular values of low and middle frequency region of host are chosen for watermark embedding using different column and row wavelet transforms is compared in Figure 8 and Figure 9.

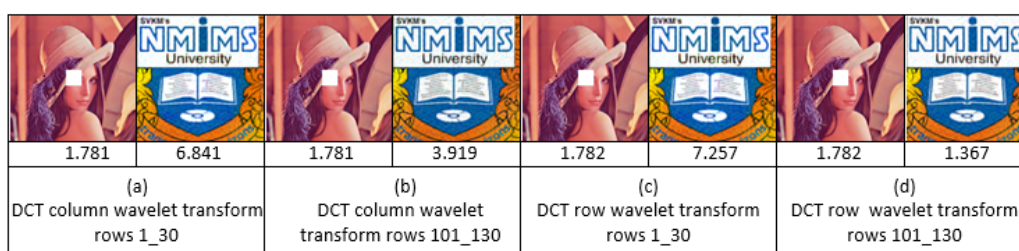


Figure 7 watermarked images after performing cropping attack and watermark extracted from them (a) when watermark is embedded in low frequency band of DCT column wavelet transform (b) when watermark is embedded in middle frequency band of DCT column wavelet transform (c) when watermark is embedded in low frequency band of DCT row wavelet transform (d) when watermark is embedded in middle frequency band of DCT row wavelet transform.

From Figure 7, it can be seen that embedding watermark in low frequency region is less robust against cropping attack than embedding in middle frequency singular values. Further, for middle frequency embedding, row DCT wavelet is more robust than column wavelet.

Figure 8 shows the comparison of performance against cropping attack when column wavelet transforms are used.

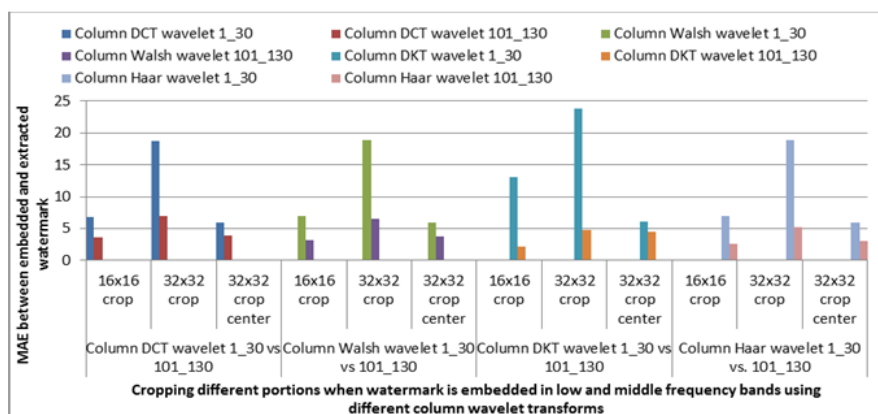


Figure 8 Comparison of MAE between embedded and extracted watermark against cropping when watermark is embedded in low and middle frequency elements using different column wavelet transforms

From Figure 8 it is observed that, all column wavelet transforms explored in proposed technique give outstanding robustness against cropping attack when watermark is embedded in middle frequency region. Comparatively, when watermark is embedded in low frequency region, robustness is less. For 32x32 cropping done at corners of an image, embedding watermark in low frequency region does not give acceptable robustness. However if we compare 16x16 cropping at corners and 32x32 cropping at center where area cropped from watermarked image is same, proposed technique shows marginally better robustness for cropping done at corners for all wavelet transforms.

Figure 9 shows comparison against cropping attack when row wavelet transforms are used to embed the watermark in low and middle frequency regions.

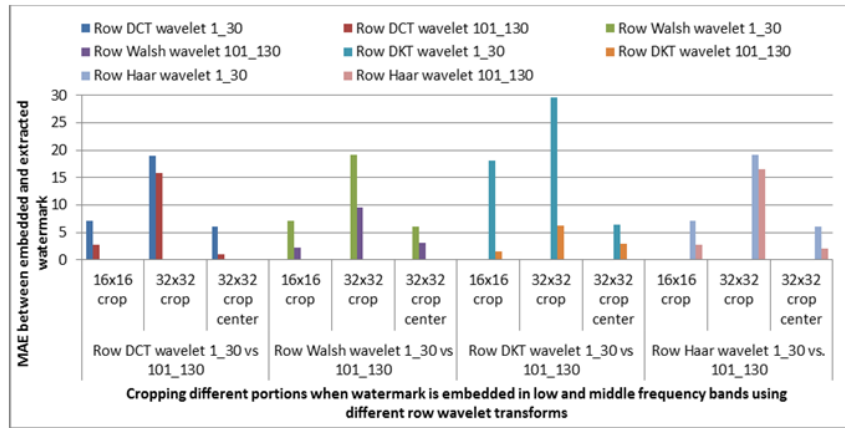


Figure 9 Comparison of MAE between embedded and extracted watermark against cropping when watermark is embedded in low and middle frequency elements using different row wavelet transforms

From Figure 9, it is observed that proposed watermarking technique is not giving good robustness for 32x32 cropping done at corners of an image using low as well as middle frequency band for embedding watermark when row DCT wavelet and row Haar wavelet is used. Row Walsh wavelet and row DKT wavelet give very good robustness against 32x32 cropping at corners and when middle frequency region is used to embed the watermark. For 16x16 cropping at corners and 32x32 cropping at center where same amount of information is cropped from image, all row wavelet transforms show excellent robustness irrespective of frequency band used for embedding. Among them row DCT wavelet and Row Haar wavelet perform marginally better for cropping at center and row Walsh and row DKT show marginally better robustness for 16x16 cropping at corners.

5.3 Noise addition to watermarked images

Binary distributed run length noise with different run length and Gaussian distributed run length noise are added to watermarked images.

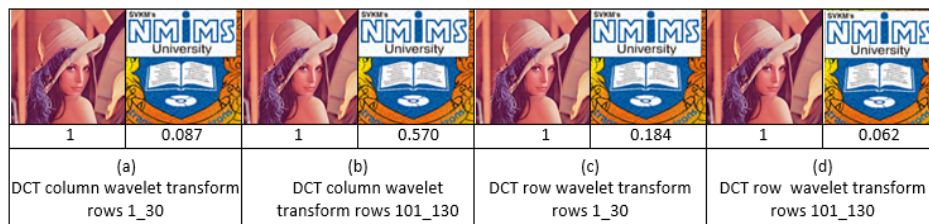


Figure 10 watermarked images after adding binary distributed random noise with run length 10 to 100 and watermark extracted from it when (a) watermark is embedded in low frequency band of column DCT wavelet transform (b) watermark is embedded in middle frequency band of column DCT wavelet transform (c) Watermark is embedded in low frequency region of row DCT wavelet transform (d) watermark is embedded in middle frequency region of row DCT wavelet transform.

Figure 11 shows the comparison of MAE between embedded and extracted watermark from different types of noise added watermarked images and when low and middle frequency singular values of host are selected for watermark embedding using column wavelet transforms.

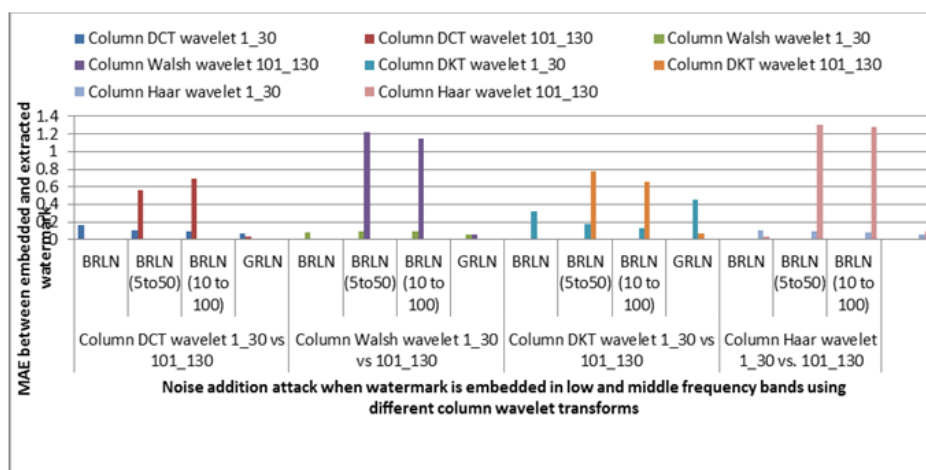


Figure 11 Comparison of MAE between embedded and extracted watermark against noise addition attack when watermark is embedded in low and middle frequency elements using different column wavelet transforms

From Figure 11 we can observe that irrespective of the frequency band selected for embedding watermark (low/middle) and column transform used for embedding process, proposed technique shows excellent robustness against noise addition attack as the MAE values between embedded and extracted watermark are very small.

Figure 12 shows comparison of low frequency and middle frequency embedding using row wavelet transforms against noise addition attacks.

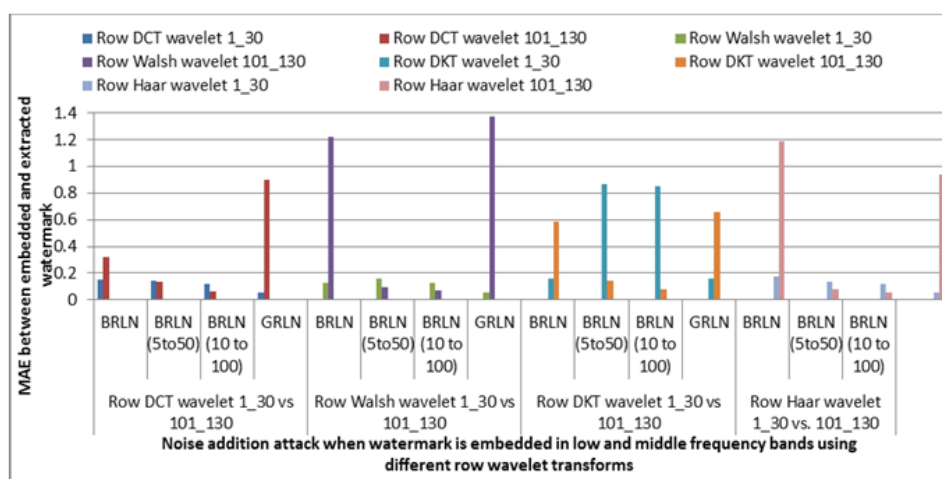


Figure 12 Comparison of MAE between embedded and extracted watermark against noise addition attack when watermark is embedded in low and middle frequency elements using different row wavelet transforms

From Figure 12 we can conclude that for binary distributed run length noise with run length 1 to 10 and for Gaussian distributed run length noise, better robustness is observed for low frequency singular values selected for watermark embedding. For increased run length of binary distributed run length noise, selection of middle frequency region to embed the watermark is more robust. Highest robustness is observed for binary distributed run length noise with run length 10 to 100 by

column DCT wavelet and column Haar wavelet when watermark is embedded in middle frequency region. For Gaussian distributed run length noise attack though for middle frequency region MAE value is higher than low frequency region, since these values itself are very small, performance of proposed technique can be considered excellent using row wavelet transforms as well.

5.4 Resizing attack

In resizing attack, watermarked image is increased in size two times and then reduced to its original size. For this bicubic interpolation, transform based image zooming [25] and grid based interpolation [26] mechanism are used. For bicubic interpolation, resizing is performed by increasing the image size to four times and two times separately and then reducing it back to original size. Figure 13 shows resized-reduced (twice large and reduced) watermarked imaged using bicubic interpolation

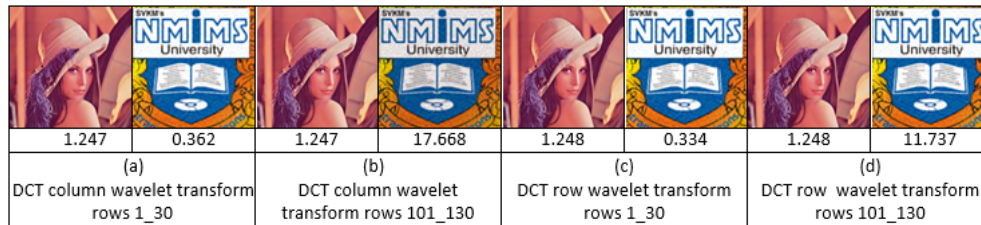


Figure 13 Watermarked images resized and reduced back to original size using bicubic interpolation and watermark extracted from them when (a) watermark is embedded in low frequency band using column DCT wavelet transform (b) watermark is embedded in middle frequency region using column DCT wavelet (c) watermark is embedded in low frequency region using row DCT wavelet transform (d) watermark is embedded in middle frequency region using row DCT wavelet.

As can be seen from Figure 13, embedding watermark in low frequency region of host is more robust against resizing attack. Average performance of various column wavelet transforms against noise addition attack when low and middle frequency regions are used to embed watermark is compared in Figure 14

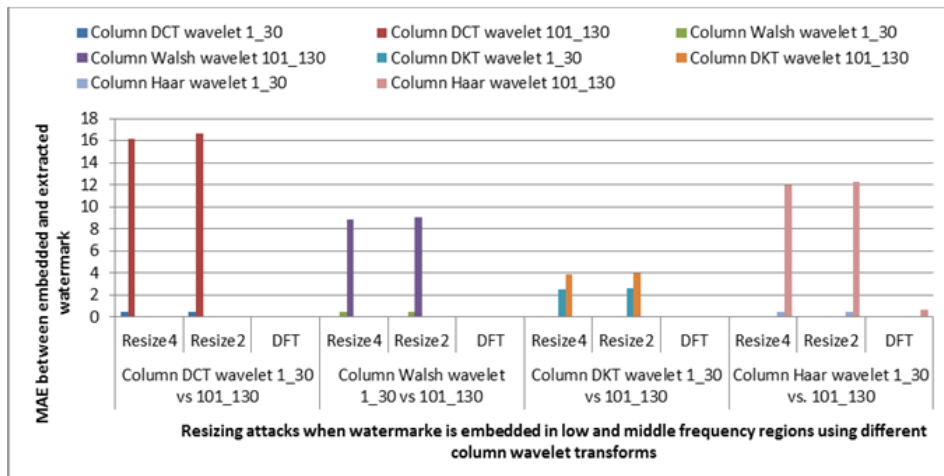


Figure 14 Comparison of MAE between embedded and extracted watermark against resizing attack when watermark is embedded in low and middle frequency elements using different column wavelet transforms

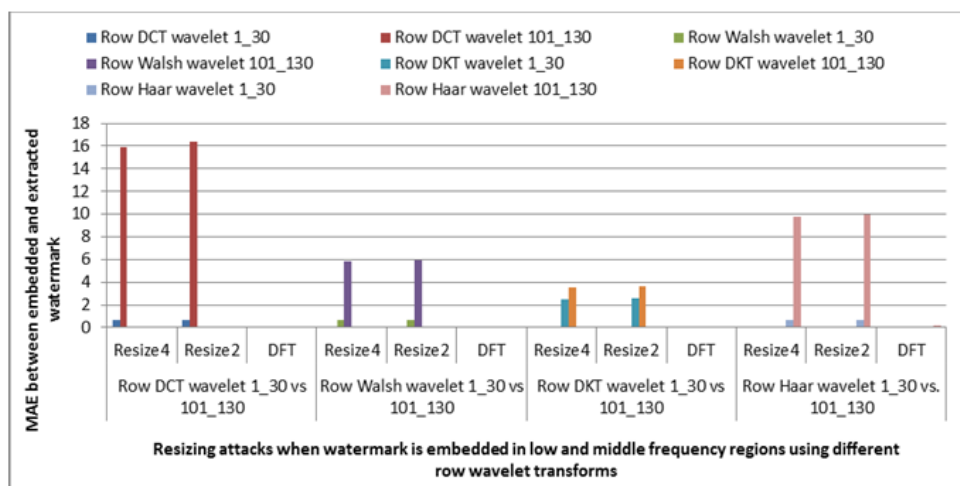


Figure 15 Comparison of MAE between embedded and extracted watermark against resizing attack when watermark is embedded in low and middle frequency elements using different row wavelet transforms

As can be seen from Figure 14 and Figure 15, different column and row wavelet transforms perform very well against bicubic interpolation based resizing attack when singular values of low frequency region of host are selected for embedding watermark. Except column DCT wavelet, other wavelet transforms also show very good robustness against bicubic interpolation attack when singular values of middle frequency region are used to embed the watermark. Also against transform based resizing and grid based resizing attack, irrespective of low or middle frequency region and transform used for embedding watermark, zero MAE is obtained between embedded and extracted watermark thus leading to excellent robustness.

Performance of proposed method against various attacks is summarized in the Figure 16. Yellow color of a node in the hierarchy indicates excellent performance, Pink indicates very good robustness and orange color indicates good robustness.

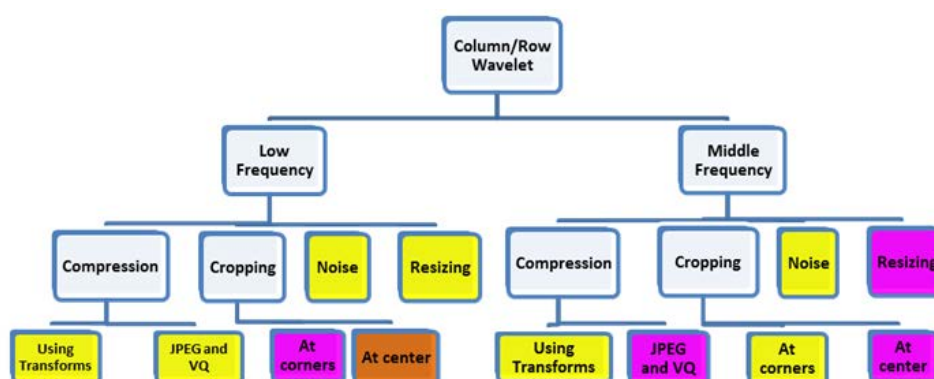


Figure 16 Summarized performance of proposed watermarking technique against various attacks (Yellow=Excellent, Pink=Very Good, Orange=Good)

6 Conclusion

Proposed method of watermarking embeds singular values of watermark in singular values of column wavelet or row wavelet transform of host. Watermarked image is subjected to different attacks and watermark is extracted from it. Selection of low frequency band proves to be robust for attacks except cropping attack. Proposed method allows embedding watermark in low frequency

region which otherwise leads to heavy distortion in watermarked image. Robustness of technique where watermark is embedded in middle frequency band is also acceptable but it is not as good as lower frequency bands.

REFERENCES

- [1]. Mingli Zhang, Qiang Zhang, Changjun Zhou, Robust Digital Image Watermarking in DWT-SVD Domain. Artificial Intelligence and Computational Intelligence Lecture Notes in Computer Science Volume 7003, 2011, pp 75-84.
- [2]. Qiang Li, Chun Yuan, Yu-Zhuo Zhong, Adaptive DWT-SVD Domain Image Watermarking Using Human Visual Model. In IEEE Proc. of the 9th International Conference on Advanced Communication Technology, 2007 (Volume:3), pp. 1947 – 1951.
- [3]. Bhagyashri Kapre, M.Y. Joshi, All frequency band DWT-SVD robust watermarking technique for color images in YUV color space. In Proc. of IEEE International Conference on Computer Science and Automation Engineering, 2011, (Volume:3), pp. 295-299.
- [4]. Erkan YAVUZ, Ziya TELATAR, Improved SVD-DWT Based Digital Image Watermarking against watermark ambiguity. In Proc. of ACM symposium on Applied computing, 2007, pp. 1051-1055.
- [5]. Ambika Agarwal, Neha Bora, Nitin Arora, Goodput enhanced digital image watermarking scheme based on DWT and SVD. International Journal of Application or Innovation in Engineering & Management, 2013, volume 2, Issue 9, pp. 36-41.
- [6]. Saeed K. Amirgholipour, Ahmad R. Naghsh-Nilchi, Robust Digital Image Watermarking Based on Joint DWT-DCT. International Journal of Digital Content Technology and its Applications, 2009, pp. 42-54.
- [7]. Surya Pratap Singh, Paresh Rawat, Sudhir Agrawal, A Robust Watermarking Approach using DCT-DWT. International Journal of Emerging Technology and Advanced Engineering, 2012, volume 2, issue 8, pp. 300-305.
- [8]. Ali Al-Haj, Combined DWT-DCT Digital Image Watermarking. Journal of Computer Science 3 (9), 2012, pp. 740-746.
- [9]. S S Bedi, Ashwani Kumar, and Piyush Kapoor, Robust Secure SVD Based DCT – DWT Oriented Watermarking Technique for Image Authentication. International Conference on IT to Celebrate S. Charmonman's 72nd Birthday, March 2009, pp. 46.1-46.7
- [10]. V. Santhi, N. Rekha , S.Tharini, A Hybrid Block Based Watermarking Algorithm using DWT-DCT-SVD Techniques for Color Images. In Proc. of international conference on computing, communication and networking, 2008, pp. 1-7.
- [11]. Zhen Li, Kim-Hui Yap, Bai-Ying Lei, A new blind robust image watermarking scheme in SVD-DCT composite domain. 18th IEEE International Conference on Image Processing (ICIP), 2011, pp. 2757 – 2760.
- [12]. Navas K.A., Ajay M.C., Lekshmi M., Archana T.S., Sasikumar M., DWT-DCT-SVD based watermarking. In Proc. of International conference on Communication Systems Software and Middleware and Workshops, 2008, pp. 271-274.

- [13]. Divecha and Jani, Implementation and performance analysis of DCT-DWT-SVD based watermarking algorithms for color images. *International Conference on Intelligent Systems and Signal Processing (ISSP)*, 2013, pp. 204 – 208.
- [14]. Pachauri S., Mehra N., Shandilya M., Attacks resistant hybrid watermarking scheme. In *Proc. of Fourth International Conference on Computing, Communications and Networking Technologies (ICCCNT)*, 2013, Page(s): 1 – 5.
- [15]. Lagzian, S. Soryani, M. Fathy, M., Robust watermarking scheme based on RDWT-SVD: Embedding data in all sub bands. *International Symposium on Artificial Intelligence and Signal Processing (AISP)*, June 2011, 48 – 52.
- [16]. Wei Cao, Yixin Yan, Shengming Li, Robust Image Watermarking Based on singular value decomposition in DT-CWT domain. *IEEE International Workshop on Imaging Systems and Techniques*, 2009, pp. 381-384.
- [17]. Wei Wang, Aidong Men, Bo Yang, Xiaobo Chen, A novel robust zero watermarking scheme based on DWT and SVD. In *Proc. of 4th international conference on Image and Signal Processing (CISP)*, 2011, pp. 1012 – 1015.
- [18]. Akshay Kumar Gupta and Mehul Raval, A robust and secure watermarking scheme based on singular values replacement. *Sadhana, Indian Academy of Sciences*, August 2012, Vol. 37, Part 4, pp. 425–440.
- [19]. Deb Kaushik, Al-Seraj Md. Sajib, Kowsar Mir Md. Saki, Sarkar Iqbal Hasan, A joint DWT-DCT based watermarking technique for avoiding unauthorized replication. *7th International Forum on Strategic Technology (IFOST)*, 2012, pp. 1 – 5.
- [20]. Krzysztof Simek, Properties of SVD based dynamical model of gene expressing data. *International Journal of Applied Maths Computer Science*, 2003, Vol. 13, No. 3, pp. 337-345.
- [21]. Cao, Lijie, Singular value decomposition applied to digital image processing, *Division of Computing Studies, Arizona State University Polytechnic Campus, Mesa*, (2006).
- [22]. Ruizhen Liu, Tieniu Tan, A SVD based watermarking scheme for protecting rightful ownership. *IEEE transactions on multimedia*, 2002, vol. 4, pp.121-128.
- [23]. Kekre, H. B., Archana Athawale, Dipali Sadavarti, Algorithm to Generate Wavelet Transform from an Orthogonal Transform. *International Journal of Image Processing (IJIP)* 4.4 (2010), pp.444-455.
- [24]. Kekre, H. B., and Tanuja K. Sarode, Fast Codebook Generation Algorithm for Color Images using Vector Quantization. *International Journal of Computer Science and Information Technology* 1.1 (2009): pp. 7-12.
- [25]. Dr. H. B. Kekre, Dr. Tanuja Sarode, Shachi Natu, Image Zooming using Sinusoidal Transforms like Hartley, DFT, DCT, DST and Real Fourier Transform. *International journal of computer science and information security* Vol. 12 No. 7, July 2014, pp. 11-16.
- [26]. H. B. Kekre, Tanuja Sarode, Sudeep Thepade, Grid based image scaling technique. *International Journal of Computer Science and Applications*, 2008, Volume 1, No. 2, pp. 95-98.

New Hybrid Approach for Identification of Spermatozoa in Human Semen Sample using Microscope Image Processing Techniques

¹Nandini M. Chaudhari and ²B. V. Pawar

North Maharashtra University, Jalgaon, Maharashtra, India

¹nandini113@yahoo.co.in, ²bvpawar@gmail.com

ABSTRACT

Due to very hectic, stressful and exhaustive life style, Today, Infertility is a common problem in most of the couples and they have to undergo for intrauterine insemination (IUI) or In-vitro fertilization (IVF). Semen analysis is fundamental test in the clinical work up of the infertile male. Computerized semen test will give many more & accurate parameters that are useful to the fertility specialist. This paper focuses on finding the numbers of spermatozoa contain in the semen sample with new hybrid approach using MATLAB. Use of background subtraction is the first stage of algorithm. Region based segmentation finds the numbers of sperm in the semen sample. The comparative analysis of segmentation shows that region base segmentation detects more objects. So it is possible to find the suppressed (low intensity) sperm in given frame.

Keywords: Semen analysis, region segmentation, spermatozoa, WHO scan line algorithm

1 Introduction

A Semen analysis is a routine pathological test which has an important role in the human reproduction. This test finds some of physical and chemical parameters. A semen analysis evaluates certain characteristics of a male's semen and the sperm contained in the semen. A routine analysis of a given ejaculate includes the evaluation of sperm concentration, motility, morphology, and vitality etc.

Some of the parameters that are calculated through microscope manually which include:

- Sperm count (technically it is the concentration) is the number of sperm in the semen sample
- Motility is the percentage of sperm those are moving in the sample. According to speed of the sperm they are classified into Type A (fast and progressive), Type B (slow progressive), Type C (Non-progressive) , Type D (immobile)
- Morphology is the shape or structure of spermatozoa

The normal values of semen parameters are referred from the manual of World Health Organization (WHO). As per WHO manual 4th & 5th edition, normal values of semen are slight variable and are shown in Table 1[1][2].

Table 1: Standard values of Semen analysis as per WHO

	WHO 1999 4th Edition	WHO 2011 5th Edition
Volume	2 ml	1.5 ml
Concentration	20 million /ml	15 million /ml
Progressive motility	50%	32%
Normal form	14%	4%

Computer assisted semen analysis (CASA) plays a vital role for the assessment of sperm concentration (counts) and motility (movement) characteristic. Most of the CASA analyzers are based on different techniques on image analysis. Various CASA system like Cell Soft (Cryo Resources Ltd, NY), Hamilton Thorne (Hamilton Thorne Research Inc, Danvers, MA) etc are used widely all over. Different technology, platforms and algorithms were embedded into different CASA systems.

Early CASA system uses signal processing technology to find the density of the semen. Lukasz Witkowski, Poland, in 2002, examine the density and trajectories of the cell movement using dilation and erosion techniques and the algorithm was developed in PASCAL [3] [4]. Since sperm finding is the first step in semen analysis it is needed to detect the individual sperm which are identified even in low contrast images. Vahid et. al. had proposed the tracking & fitting algorithm in MATLAB to identify the individual complete (head & tail) spermatozoa as an elliptical shape in 2005 [5]. Henry Corriolo et.al. [6] was focused on finding the features of spermatozoa. The method called nth-fusion was introduced in his work, the framework of the segmentation algorithm for region of interest head, Acrosome, Nucleus and Mid-piece was segmented.

J.M.Pascual-Gaspar et. al. [7] in 2008 had proposed a simple and effective system for computer assisted semen analysis took lot of efforts to evaluate the density of semen and motility of individual spermatozoa by using simple but effective computer vision techniques.

Hiromasa Oku et al. [8] reported a new automatic visual tracking system for small, fast-moving objects using high-speed visual feedback. He achieved stable tracking of fast, small ascidian spermatozoa for more than 180 s using high-speed visual feedback. The two stage algorithm proposed by Abhirramy focused on the motion detection and motion tracking of spermatozoa with some preprocessing operations like image enhancement using Laplacian filter & median filtering. Most basic morphological operations like dilation, erosion and thresholding using gradient operators Sobel & Edge. Features of identified objects was stored and labeled them accordingly. Identified spermatozoa were tracked in each frame [9]. The review on techniques of CASA for semen analysis indicates that Pathologist and microbiologist need a manual cum standard computer assisted, cost effective semen analyzer with optimal result, since semen analysis is now routine checkup for infertile couples. [10]

2 Microscope Image Processing Techniques

Techniques employed for processing microscopy images are in general rather different from those encountered in consumer image processing. Most applications will have a suite of standard operations such as sharpening, contrast and brightness enhancement, and color balancing.

One key requirement is to remove the distortion in optical path microscope & blurring caused by instrumentation.

2.1 Image subtraction

Image subtraction is an image correction techniques and calibration methods for both image visualization and quantitative analysis.

Image subtraction is usually performed when two images of the same object are obtained under different conditions. The image subtraction will highlight whatever has changed between the two images. Another application is background correction. In microscopic imaging the image is often affected by a slowly varying background shading pattern. One can move the microscope stage to an empty field and acquire an image of the background. When the background image is subtracted from the image containing the specimen, it removes the shading.

$$I_{\text{work}}(x, y) = I_{\text{speciman}}(x, y) - I_{\text{back}}(x, y)$$

Where $I_{\text{speciman}}(x, y)$ is a digital image produced by the microscope, $I_{\text{back}}(x, y)$ is a background image produced by low-pass filtering the specimen image to smooth, where the smoothing effect is larger than the size of objects in the image [11].

2.2 Region based segmentation

The main aim of segmentation is the division of digital image into group of connected pixels with identical properties i.e. region which is easier to analyze. There are three general approaches for segmentation: Edge, Boundary and Region. In edge based segmentation it finds all pixels on region on boundary i.e. divide into edge and non-edge pixels. Region based segmentation, works repetitively by grouping pixel together which are neighbors (4-connectivity or 8-connectivity) and have same values. Boundary based segmentation pixels are marked on the basis of range of value in which pixel lies.

3 Proposed Hybrid Image Processing Approach to Detect the Spermatozoa

Since the sperms are rapid motile, it is very difficult to count the number of sperm manually, but by capturing them in video and then count is easy way. So we have proposed a new system in which the frames extracted from recorded video is used as an input to the proposed system. We have called it a hybrid approach since after identifying the moving object, scan line algorithm is applied for confirmation of the objects having tails, so that we can count the actual number of spermatozoa. The standard data set was prepared from the different semen samples. For testing the efficiency of proposed algorithm, same frames were applied to the existing algorithm.

The architectural framework for the propose hybrid system is shown in figure 1.

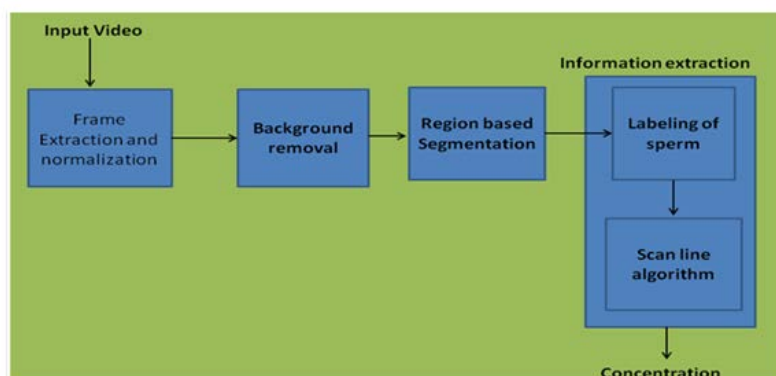


Figure 1: Proposed hybrid system

The propose algorithm contains the following steps-

- Frame extraction & Normalization
- Background creation & subtraction for background removal
- Region based sperm detection
- Information extraction
- Find concentration i.e. No of sperms

By using the background subtraction technique the algorithm find the objects. By avoiding the preprocessing steps we have improved the computation of the algorithm. Region based segmentation with region to be connected as 4-connect is used to find the area of interest that may an object which has sperm data. Actual spermatozoa are identified by detecting the tail of the sperm. So before finding the concentration we need to check whether the identified object had tail with help of scan line algorithm.

3.1 Frame extraction & Normalization

3.1.1 Experimental video setup

Most of the pathological laboratories are doing semen analysis by measuring the sperm concentration, motility, vitality by manual method as shown in figure 2a. In most of the cases, sperm concentration and motility are improved manually using nebular counting chamber, Makler Chamber. Makler chamber is a counting chamber Medical instrument for microscope which allows you to count the sperm chamberwise. Setting up the video setup with microscope the frame can be extracted with the recorded video as shown in figure 2b with help of video to s-video adapter with the block diagram as shown in figure 2c. Microscope is LABOMED make LED cluster with UPS & SMF battery and AVC 561V Digital Color CCD camera with WinPvr. A video is a sequence of images or frames with time difference in second. The frames with recorded videos are converted into frames as a bitmap file with file size 352 X 576.

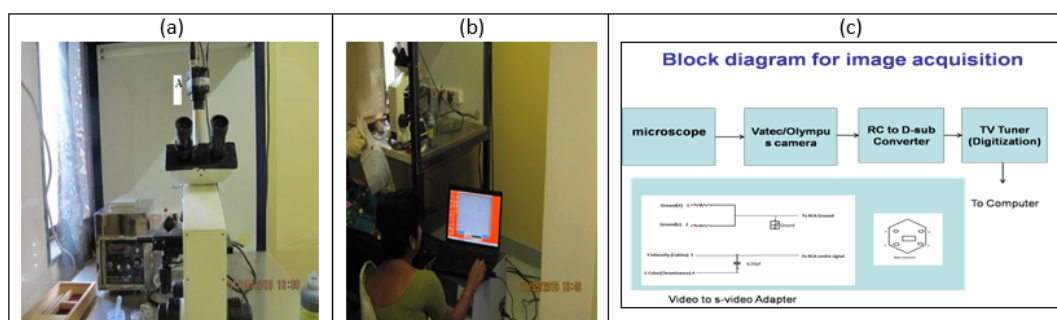


Figure 2: manual method & video setup with microscope

3.2 Background creation & subtraction for background removal

This is a first stage of the algorithm, instead of preprocessing stages and frame enhancement; we have created the background and remove the background from all frames, which is created from the first frame. Background subtraction is done pixel by pixel. The background image is created from the first frame of the video. Process for extraction if the difference Dvalue is satisfying predefined threshold.

```

Algorithm:
Background removal using background subtraction
[Input]: Frames Fn. {F1, F2, F3 ...Fn}
[Output]: Region nm obtained from each frame
Where n is frame no & m is a no of sperms in individual
frames.
Pick the background image say Bk
For i= 1 to n
Dvalue ← Fi-Bk Where n is the no. of frames to be
processed
If (Dvalue <= Threshold)
Dvalue=0
else
Extract the region of interest (ROI) whose min area is> 4.
End
Stop
    
```

3.3 Region based sperm detection

3.3.1 Why region based segmentation?

The numbers of objects detected in region based segmentation technique are more due to the intensity difference of region as shown in figure 3. But here we can find the sperms which are at lower level may be not having very good intensity and cannot visualize by naked eyes. So the chances of finding number of sperm can be more by checking the region of interest as shown in table 2, by verifying whether the ROI contains sperm data we can label the object.

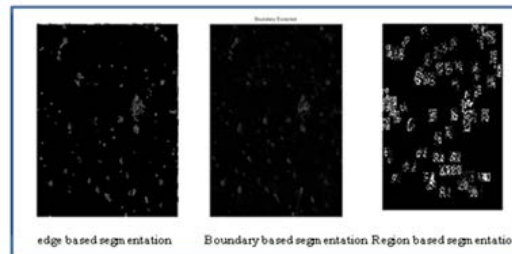


Figure 3: result of different segmentation techniques

Table 2: no of ROI generated by segmentation techniques

Frame number	Methods type		
	Edge based	Boundary based	Region based
1	800	423	1339
2	812	362	4983
3	818	350	2999
4	813	377	5255
5	806	374	5520
6	808	355	4749
7	817	386	6033
8	816	371	6140
9	806	354	5664
10	836	369	6946

By avoiding the preprocessing steps we can improve the computation of the algorithm. Region based segmentation with region to be connected as 4-connect is used to find the area of interest that may an object which has sperm data.

```
Algorithm: Region based sperm detection
Convert current instance of frame to grayscale
Label 4-connect component
After Applying region based segmentation measure
the properties of contiguous regions.
Extract the region of interest (ROI) whose min area
is 4.
Extracting all the parameter into the detector
region into the form of file & in cell data structure a
structural array.
```

3.4 Information extraction

There are two stages in this step, one is labeling of the object and check if tail exists in the detected region so as it is a sperm. First Detect the bounding box value of each detector region, crop the image & Check whether it contain sperm data. The identified objects from first five frames are labeled and are shown in figure 4.

```
[Input]: Information of detected region in individual
frames
[Output]: Structural array contains sperm information

Part1 Labeling of sperm

Here the tail information is extracted and the sperm is
labeled and detect its variations in all frames.
For i= 1 to m
  r ← Ri Where m is the total no. of region
  obtained
For j = 1 to n Where n is no. of frames
  r' ← Rij Where Rij is a region of its order in frame j.

  If (r-r' < threshold)
    Accept it as a same region
  else
    reject r' and calculate its variations(v) &
    distance(d)
    [v,d] ← calculate (r')
    r[v,d] ← [v,d]
End
End
Sc < r then c++
Stop
```

3.5 Find concentration i.e. No of sperms

After extraction of information and storing it in mat file we need to check for the redundancy to find the actual number of sperms exists in the semen sample. Load the .mat file and compare the current file to next file. If the parameters are same then the same sperm is detected, we need to find the variation of the centroid otherwise store it as another sperm and count.

```
[Input] .mat file generated for individual sperm in each
frame
[Output] Count the number of sperm as a concentration
For i=1 to total .mat file
Load current .mat file
Load next .mat file file1
Compare sperm parameters of file and file1
If equal
  The sperm is detected in next frame, find its variation
Else
  Count=count+1
End
```


4 Experiments, Results & Discussion

4.1 Comparative study

With setting up the microscope with video setup as shown in figure1 & extracting the frames at the rate of 25 FPS, we are trying to find the concentration of the raw semen sample. A proposed hybrid approach shows that detected labeled objects are more accurate than the existing system. The sperm which are not detected in the current frame gets detected in the next frame as shown in figure 4, So the chances for finding the more number of correct sperms. The number of object labeled in Table 3 shows that the accuracy for labeling of sperm by our proposed approached is near by the manual method. Figure5 indicates that the percentage of accuracy for labeling of the object is nearly 93.18%.

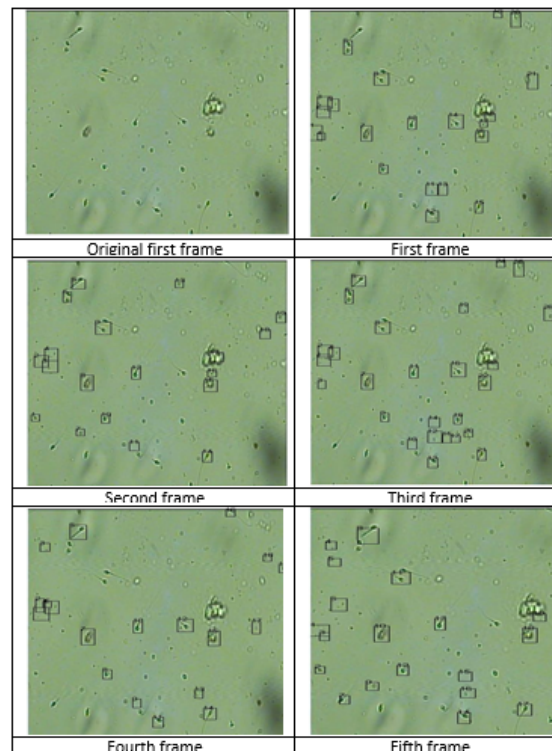


Figure 4: labeling of the sperm

Table 3: Actual no of labeled objects

Frame No	Manual Method	Existing algorithm	Proposed Hybrid algorithm
1	20	39	21
2	19	41	19
3	17	40	26
4	20	41	19
5	22	45	22

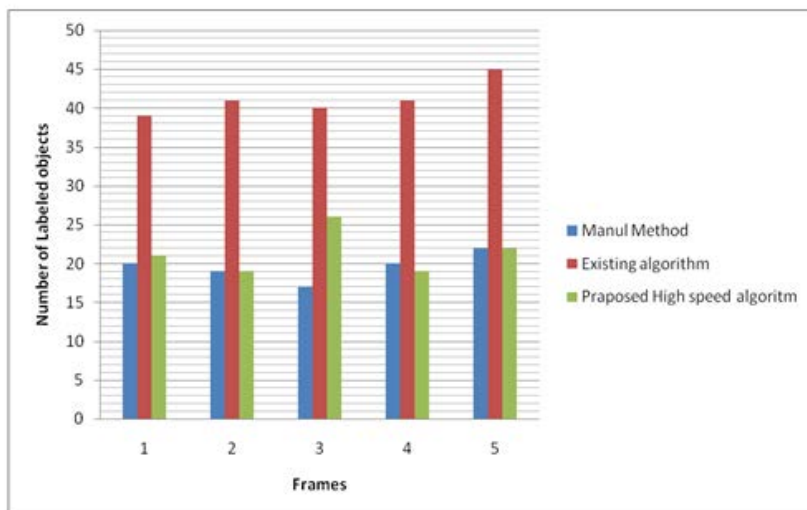


Figure 5: Graph for Comparison graph of labeled objects in different method

4.2 Performance Evaluation

Evaluation of the proposed system is based on the performance measure for the rate of false positive, false negative, sensitivity, specificity & accuracy. Accuracy allows us to measure how well binary classification of detected sperms and non-detected sperms tests correctly identified or excludes. It is a proportion of true results for both true positive and true negative in the identified spermatozoa. The classification of TP, TN, FP, and FN are shown according to table 4.

Table: 4 Classification criteria for labeled objects

Labeled objects	Sperms	Debris/Artifacts
Detected object	TP	FP
Not detected object	TN	FN

According to above table the labeled spermatozoa, the accuracy, sensitivity and specificity can be calculated as

$$\text{Accuracy} = \frac{\text{True Positive} + \text{True negative}}{\text{True Positive} + \text{True negative} + \text{False Positive} + \text{False negative}}$$

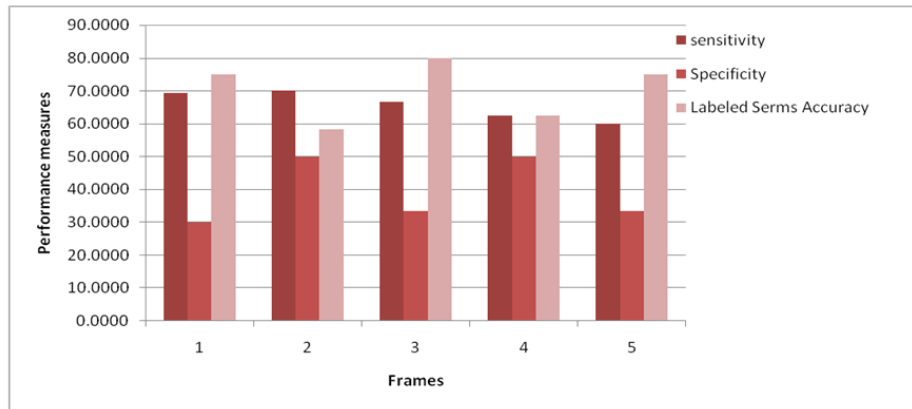
$$\text{Sensitivity} = \frac{\text{True Positive}}{\text{True Positive} + \text{False negative}}$$

$$\text{Specificity} = \frac{\text{True negative}}{\text{True negative} + \text{False Positive}}$$

The no of true positive labeled is considered as a spermatozoa , As compared with the area and perimeter of the true spermatozoa the artifacts or debris are classified as a false negative and false positive. According the outcome of percentage of accuracy, sensitivity and specificity are tabularized in Table 5. The overall labeled sperms average accuracy is up to 70%. So as per discussion with experts to find semen analysis it is considered as a 100 percentile. So according to our proposed method the percentile varies in the range of 80% to 100%. The evaluation of these performance measures are shown in figure 6 in graphical format.

Table 5: Evaluation of the proposed hybrid approach

Frame No	No. of labeled object	Total sperm in the frame	detected sperm (TP)	Not detected sperm (TN)	non detected artifacts(FN)	detected artifacts as sperm (FP)	Accuracy	sensitivity	Specificity	Labeled Sperms Accuracy
1	21	12	9	3	4	7	0.5217	69.2308	30.0000	75.0000
2	19	12	7	5	3	5	0.6000	70.0000	50.0000	58.3333
3	26	10	8	2	4	4	0.5556	66.6667	33.3333	80.0000
4	19	8	5	3	3	3	0.5714	62.5000	50.0000	62.5000
5	22	8	6	2	4	4	0.5000	60.0000	33.3333	75.0000

**Figure 6: The evaluation of these performance measures**

5 Conclusions

The number of objects (spermatozoa) detected by our hybrid approach for spermatozoa detection algorithm are at par as per the manual method with 83% of frame wise labeling. In this paper region based segmentation and scan line algorithm helps in finding the object as a sperm which are at lower level with low intensity and so the concentration. This is achieved without using any preprocessing operation like image enhancement. The overall labeled sperms with tails the accuracy percentage is 70%.

Acknowledgement

The authors are thankful to the University Grants Commission, New Delhi for supporting this research under the Special Assistance Programme (SAP) at the level of DRS-I (No: F.3-52/2011(SAP-II)).

REFERENCES

- [1]. Kevin Coetzee, Thinus F.Kruger and Carl J.Lombard, "Predictive value of normal sperm morphology: a structured literature review", Human Reproduction Update 1998, Vol. 4, No. 1 pp. 73–82
- [2]. WHO Laboratory manual for the examination of human semen and sperm-cervical mucus interaction. World Health Organization, 4th ed., Cambridge University Press, 1999.
- [3]. Lukasz Witkowski , " Exam of the density of semen and analysis of sperm cell movement ",Journal of medical informatics & technology, Vol 3/2002 , ISSN 1642-6037 .
- [4]. Lukasz Witkowski , " An automatic system for calculating basic semen parameter" , TASK QUARTERLY 8 No 2 (2004), 231–236 .

- [5]. Vahid Reza Nafisi, Mohammad Hasan Moradi, and Mohammad Hosain Nasr-Esfahani , “ Sperm Identification Using Elliptic Model and Tail Detection”, *World Academy of Science, Engineering and Technology* ,6 2005.
- [6]. Henry Carrillo, Jorge Villarreal, Miguel Sotaquirá ,colombia , ” Spermatozoon Segmentation Towards an Objective Analysis of Human Sperm morphology”, *Proceedings of the 5th International Symposium on image and Signal Processing and Analysis* (2007).
- [7]. J. M.Pascual-Gaspar, H. Olmedo, A.I. Exposito , A. Exposito³ and J.Finat¹ , Spain, “A simple and effective system for Computer Assisted Semen Analysis “,*Advances in Medical signal and information processing* , 2008, 4th International conference, Santa Margherita Ligure, Italy, ISBN:9780 86341 934 8, 14-16 July 2008 .
- [8]. Hiromasa Oku and Masatoshi Naoko Ogawa Kogiku Shiba andManabu , japan , “How to Track Spermatozoa using High-Speed Visual Feedback “,*30th Annual International IEEE EMBS Conference* , Vancouver, British Columbia, Canada, August 20-24, 2008 .
- [9]. V.S.Abbiramy et. Al.,“Spermatozoa Detection, Counting and Tracking in Video Streams to Detect Asthenozoospermia “, *2010 International Conference on Signal and Image Processing*.
- [10]. Chaudhari, N.M.; Pawar, B.V., "Light scattering study on semen analysis methods/techniques," *Engineering (NUICONE)*, 2013 Nirma University International Conference on Engineering, vol., no., pp.1,4, 28-30 Nov. 2013.
- [11]. Qiang Wu, Fatima A. Merchant, Kenneth R. Castleman, *Microscope Image Processing*, Academic Press, United States of America, 2008.

Medical Image Compression using DCT and DWT Techniques

Gullanar M. Hadi

*College of Engineering-Software Engineering Dept.
Salahaddin University-Erbil, Iraq
gullanarm@yahoo.com*

ABSTRACT

In this paper we used DCT (Discrete Cosine Transform) and DWT (Discrete Wavelet Transform) to achieve optimal compression ratio for two types of medical images (CT scan and MRI) with keeping good quality of these images. In 2D- DCT; the image is broken up into blocks of $n \times m$ pixels p_{xy} (with $n=m= 8$ typically), and then 2D- DCT is used to produce a block of $n \times m$ DCT coefficients for each block of pixels, the result coefficients are quantized, which must result in lossy but highly efficient compression ratio . The important feature of the DCT the feature that makes it so useful in data compression, is that it takes correlated input data and concentrates its energy in just the first few transform coefficients. For the same images we used DWT method, and then compare their results to choose the best method for compressing medical image with good quality. The compression algorithms programmed and tested to achieve the goal of reducing the file size (i.e., good compression ratio) using Matlab (R2008a).The conclusion part in this paper explain the results.

Keywords: Data Compression Techniques, Image Compression, DCT, DWT, Medical images.

1 Introduction

In computer science and information theory, data compression, source coding, or bit-rate reduction involves encoding information using fewer bits than the original representation. Compression is useful because it helps reduce resources usage, such as data storage space or transmission capacity. Because compressed data must be decompressed to use, this extra processing imposes computational or other costs through decompression. Compression can be either lossy or lossless as follows: [1] [2] Lossless compression reduces bits by identifying and eliminating statistical redundancy, where redundancy in information theory is the number of bits used to transmit a message minus the number of bits of actual information in the message. Lossless data compression make use of data compression algorithms that allows the exact original data to be reconstructed from the compressed data. No information is lost in lossless compression. This can be contrasted to lossy data compression, which does not allow the exact original data to be reconstructed from the compressed data. Also lossless compression is used when it is important that the original and the decompressed data be identical, or when no assumption can be made on whether certain deviation is uncritical. Typical examples are executable programs and source code.

Some image file formats, notably PNG, use only lossless compression, while others like TIFF and MNG may use either lossless or lossy methods. GIF uses a lossless compression method, but most GIF implementations are incapable of representing full color, so they quantize the image (often with dithering) to 256 or fewer colors before encoding as GIF. Color quantization is a lossy process, but reconstructing the color image and then re-quantizing it produces no additional loss. On other hand,

WebP is a new image format that provides lossless and lossy compression for images on the web. WebP lossless images are 28% smaller in size compared to PNGs. WebP lossy images are 25-34% smaller in size compared to JPEG images. [3] Lossless data compression is used in many applications. For example, it is used in the popular ZIP file format and in the UNIX tool gzip. It is also often used as a component within lossy data compression technologies.

Lossy compression reduces bits by identifying unnecessary information and removing it. The process of reducing the size of a data file is popularly referred to as data compression, although it's formal name is source coding (coding done at the source of the data before it is stored or transmitted). A lossy data compression method is one where compressing data and then decompressing it retrieves data that may well be different from the original, but is "close enough" to be useful in some way. Lossy data compression is used frequently on the Internet and especially in streaming media and telephony applications. These methods are typically referred to as codecs in this context. Most lossy data compression formats suffer from generation loss: repeatedly compressing and decompressing the file will cause it to progressively lose quality. This is in contrast with lossless data compression.

2 Why do We Need Image Compression?

In case of image compression: As an activity, digital image processing generally creates significant numbers of large files containing digital image data. Very often, these must be archived or exchange among different users and system. This call for efficient methods for the storage and transfer of digital image data files.

-Since digital images, by their nature, are quite data intensive, reducing their size can produce solutions that are more ambitious than would otherwise be practical .by eliminating redundant or unnecessary information, Image compression is the activity that addresses this aim.

-Digital image coding and compression is concerned with the minimization of the memory needed to represent and store a digital image. And the term data compression refers to the process of reducing the amount of data required to represent a given quantity of information. It is well known that raw digital images occupy a large amount of memory. For example 1024 x 1024 color image requires 3 MB of memory for its storage (1024 x 1024 x 3 bytes /pixel).

3 Error Metrics

This article demonstrates the compression and uncompressing of a grayscale image (i.e. Medical images and other type) and computed MSE and PSNR error values using the 'spiht' compression method. See wcompress function in matlab. [5]

Two measures are commonly used to quantify the error between two images: the Mean Square Error (MSE) and the Peak Signal to Noise Ratio (PSNR) which is expressed in decibels to achieve desirable compression ratios. The MSE is the cumulative squared error between the compressed and the original image, whereas PSNR is a measure of the peak error

The mathematical formulae for the two are: [1], [4], and [5]

$$MSE = \frac{1}{mn} \sum_{i=0}^{m-1} \sum_{j=0}^{n-1} (I(i,j) - I'(i,j))^2 \quad (1)$$

$$PSNR = 20 * \log_{10} (255 / \sqrt{MSE}) \quad (2)$$

Where $I(i, j)$ is the original image, $I'(i, j)$ is the approximated version (which is actually the decompressed image) and M, N are the dimensions of the images. A lower value for MSE means lesser error, and as seen from the inverse relation between the MSE and PSNR, this translates to a high value of PSNR. Logically, a higher value of PSNR is good because it means that the ratio of Signal to Noise is higher. Here, the 'signal' is the original image, and the 'noise' is the error in reconstruction. So, if you find a compression scheme having a lower MSE (and a high PSNR), you can recognize that it is a better one. [4]

3.1 Mean Square Error (MSE)

Mean square error is a criterion for an estimator: the choice is the one that minimizes the sum of squared errors due to bias and due to variance. The average of the square of the difference between the desired response and the actual system output. As a loss function, MSE is called squared error loss. MSE measures the average of the square of the "error. The MSE is the second moment (about the origin) of the error, and thus incorporates both the variance of the estimator and its bias. For an unbiased estimator, the MSE is the variance. In an analogy to standard deviation, taking the square root of MSE yields the root mean squared error or RMSE. Which has the same units as the quantity being estimated. For an unbiased estimator, the RMSE is the square root of the variance, known as the standard error. [4]

$$MSE = \frac{1}{mn} \sum_{i=0}^{m-1} \sum_{j=0}^{n-1} \|I(i,j) - K(i,j)\|^2 \tag{3}$$

Where $m \times n$ is the image size and $I(i, j)$ is the input image and $K(i, j)$ is the retrieved image, where the simple image statistics (sample mean, and sample variance) represented as follows:

The sample mean (m_A) of an image A ($N \times M$): [6]

$$m_A = \frac{1}{mn} \sum_{i=0}^{m-1} \sum_{j=0}^{n-1} A(i,j) \tag{4}$$

$$variance = \frac{1}{mn} \sum_{i=0}^{m-1} \sum_{j=0}^{n-1} (I(i,j) - m_A)^2 \tag{5}$$

The sample standard deviation is, $\sqrt{variance}$.

3.2 Peak Signal-to-Noise Ratio (PSNR):

It is the ratio between the maximum possible power of a signal and the power of corrupting noise .Because many signals have a very wide dynamic range, PSNR is usually expressed in terms of the logarithmic decibel scale. The PSNR is most commonly used as a measure of quality of reconstruction in image compression etc. It is most easily defined via the mean squared error (MSE) which for two $m \times n$ monochrome images I and K where one of the images is considered noisy.[1],[4],[5]

$$PSNR = 10 \cdot \log_{10} \left(\frac{MAX_I^2}{MSE} \right) = 20 \cdot \log_{10} \left(\frac{MAX_I}{\sqrt{MSE}} \right) \tag{6}$$

$$PSNR = 20 * \log_{10} (255 / \text{sqrt}(MSE))$$

Here, MAX_I is the maximum possible pixel value of the image. When the pixels are represented using 8 bits per sample, this is 255. More generally, when samples are represented using linear PCM with B bits per sample, MAX_I is $2^B - 1$. Typical values for the PSNR in Lossy image and video compression are between 30 and 50 dB, where higher is better. PSNR is computed by measuring the pixel difference

between the original image and compressed image. Values for PSNR range between infinity for identical images, to 0 for images that have no commonality. PSNR decreases as the compression ratio increases for an image. For more detail see ref. [1] p/465

4 2D Discrete Cosine Transform (DCT) for Image Compression

The important feature of the DCT, the feature that makes it so useful in data compression, is that: it takes correlated input data and concentrates its energy in just the first few transform coefficients. If the input data consists of correlated quantities, then most of the n transform coefficients produced by the DCT are zeros or small numbers, and only a few are large (normally the first ones). See equation (7).

In this paper, however, we discussed image compression which is based on the two-dimensional correlation of pixels (a pixel tends to resemble all its near neighbors, not just those in its row) see equation (8). This is why practical image compression methods use the DCT in two dimensions. The image is broken up into blocks of $n \times m$ pixels (with $n=m= 8$ typically), and Equation (8) is used to produce a block of $n \times m$ DCT coefficients (DC coefficient) for each block of pixels. The coefficients are then quantized, which results in lossy but highly efficient compression. [7][8]

where

$$G_f = \sqrt{\frac{2}{n}} C_f \sum_{t=0}^{n-1} p_t \cos \left[\frac{(2t+1)f\pi}{2n} \right], \tag{7}$$

$$C_f = \begin{cases} \frac{1}{\sqrt{2}}, & f = 0, \\ 1, & f > 0, \end{cases} \text{ for } f = 0, 1, \dots, n-1$$

$$G_{ij} = \frac{2}{\sqrt{mn}} C_i C_j \sum_{x=0}^{n-1} \sum_{y=0}^{m-1} p_{xy} \cos \left[\frac{(2y+1)j\pi}{2m} \right] \cos \left[\frac{(2x+1)i\pi}{2n} \right]. \tag{8}$$

For $0 \leq i \leq n-1$ and $0 \leq j \leq m-1$ and for C_i and C_j defined by Equation (7). The first coefficient G_{00} is again termed the “DC coefficient” and the remaining coefficients are called the “AC coefficients.” The decoder reconstructs a block of quantized data values by computing the IDCT whose definition is: [7], [9]

$$p_{xy} = \frac{2}{\sqrt{mn}} \sum_{i=0}^{n-1} \sum_{j=0}^{m-1} C_i C_j G_{ij} \cos \left[\frac{(2x+1)i\pi}{2n} \right] \cos \left[\frac{(2y+1)j\pi}{2m} \right] \tag{9}$$

We now show one way to compress an entire image with the DCT in several steps as follows:

1. The image is divided into k blocks of 8×8 pixels each. The pixels are denoted by P_{xy} . If the number of image rows (columns) is not divisible by 8, the bottom row (rightmost column) is duplicated as many times as needed.
2. The DCT in two dimensions [Equation (8)] is applied to each block B_i , also see java code (figure 1).

We illustrate the performance of the DCT in two dimensions by applying it to one block of 8×8 values. The results are DCT coefficients, then quantized these coefficients after that we calculate the size of the quantized image to get compression ratio (1- compressed image size/original image size). see Table 1(a,b,c,d) [1], and the java code (figure 1) to calculate 2D DCT results.

Table 1: Two -Dimensional DCT of a Block of Correlated Data [taken from Ref. [1]]

12	10	8	10	12	10	8	11	81	0	0	0	0	0	0	0	0
11	12	10	8	10	12	10	8	0	1.57	0.61	1.90	0.38	<u>1.81</u>	0.20	<u>0.32</u>	
8	11	12	10	8	10	12	10	0	<u>0.61</u>	0.71	0.35	0	0.07	0	0.02	
10	8	11	12	10	8	10	12	0	<u>1.90</u>	<u>0.35</u>	4.76	0.77	<u>3.39</u>	0.25	<u>0.54</u>	
12	10	8	11	12	10	8	10	0	<u>0.38</u>	0	<u>0.77</u>	8.00	0.51	0	0.07	
10	12	10	8	11	12	10	8	0	<u>1.81</u>	<u>0.07</u>	<u>3.39</u>	<u>0.51</u>	1.57	0.56	0.25	
8	10	12	10	8	11	12	10	0	<u>0.20</u>	0	<u>0.25</u>	0	<u>0.56</u>	<u>0.71</u>	0.29	
10	8	10	12	10	8	11	12	0	<u>0.32</u>	<u>0.02</u>	<u>0.54</u>	<u>0.07</u>	<u>0.25</u>	<u>0.29</u>	<u>0.90</u>	
(a) Original data								(b) DCT coefficients								
81	0	0	0	0	0	0	0	12.29	10.26	7.92	9.93	11.51	9.94	8.18	10.97	
0	2	1	2	0	2	0	0	10.90	12.06	10.07	7.68	10.30	11.64	10.17	8.18	
0	1	1	0	0	0	0	0	7.83	11.39	12.19	9.62	8.28	10.10	11.64	9.94	
0	2	0	5	1	3	0	1	10.15	7.74	11.16	11.96	9.90	8.28	10.30	11.51	
0	0	0	1	8	1	0	0	12.21	10.08	8.15	11.38	11.96	9.62	7.68	9.93	
0	2	0	3	1	2	1	0	10.09	12.10	9.30	8.15	11.16	12.19	10.07	7.92	
0	0	0	0	0	1	1	0	7.87	9.50	12.10	10.08	7.74	11.39	12.06	10.26	
0	0	0	1	0	0	0	1	9.66	7.87	10.09	12.21	10.15	7.83	10.90	12.29	
(c) Quantized								(d) Reconstructed data (good)								

```
// java code to calculate 2D DCT for image A (8 x 8).
public class DCT2D {
    public static void main(String[] a) throws Exception{
        double PI=3.14159265;
        int A[][]={{12, 10, 8, 10, 12, 10, 8, 11},
                  {11, 12, 10, 8, 10, 12, 10, 8},
                  {8, 11, 12, 10, 8, 10, 12, 10},
                  {10, 8, 11, 12, 10, 8, 10, 12},
                  {12, 10, 8, 11, 12, 10, 8, 10},
                  {10, 12, 10, 8, 11, 12, 10, 8},
                  {8, 10, 12, 10, 8, 11, 12, 10},
                  {10, 8, 10, 12, 10, 8, 11, 12}};

        double G=0;
        int i,j,u,v;

        for(i = 0; i <= 7; i++) {
            for(j = 0; j <= 7; j++) {
                G = 0.0;
                for(u = 0; u <= 7; u++) {
                    for(v = 0; v <= 7; v++) {
                        double x = 1;

                        double y = 1;
                        if (i == 0)
                            x = 1/Math.sqrt(2.0);
                        if (j == 0)
                            y = 1/Math.sqrt(2.0);
                        G=G+(0.25*x*y*Math.cos(((PI*i)/(2*8))*(2*u + 1))*Math.cos(((PI*j)/(2*8))*(2*v + 1))*A[u][v]);

                        if(G<-1)
                            System.out.print("G["+i+"]"+"["+j+"]= "+(0)+"\n");
                        else
                            if(G>-1)
                                G=Math.round(G);
                                System.out.print("G["+i+"]"+"["+j+"]= "+(G)+"\n");}}
                    System.out.print("\n\n\n\n"); } }
            }
    }
}
```

Figure 1: java code to calculate 2D DCT

5 Wavelet Transform

This article demonstrates the compression and uncompression of a grayscale image (i.e. Medical images of CT and MRI types) and computed MSE and PSNR error values using the 'spiht' compression method. See wcompress function details in Matlab. [5]

Where, set partitioning in hierarchical trees (SPIHT) is an image compression algorithm that exploits the inherent similarities across the sub bands in a wavelet decomposition of an image. It is the powerful wavelet-based image compression method. The algorithm codes the most important

wavelet transform coefficients first, and transmits the bits so that an increasingly refined copy of the original image can be obtained progressively. For more details see Ref. [10].

The structure of the wavelet transform based compression is shown in figure 2 below: [9] [11]

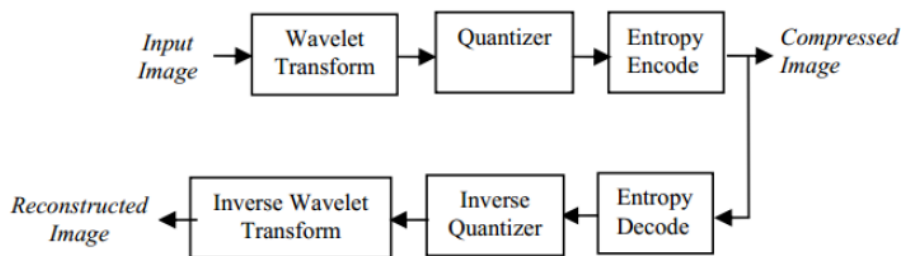
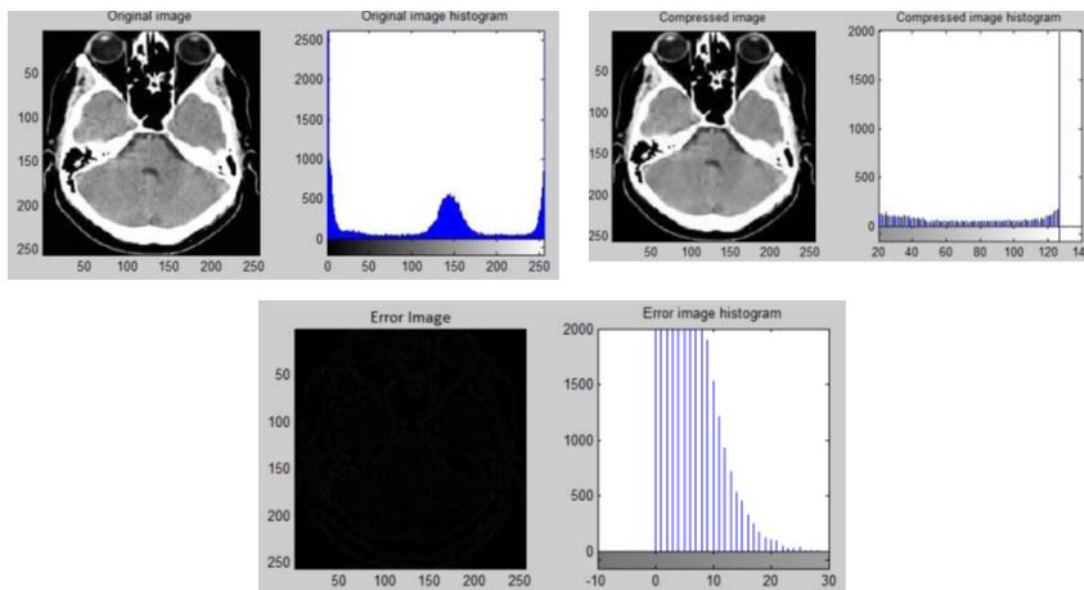


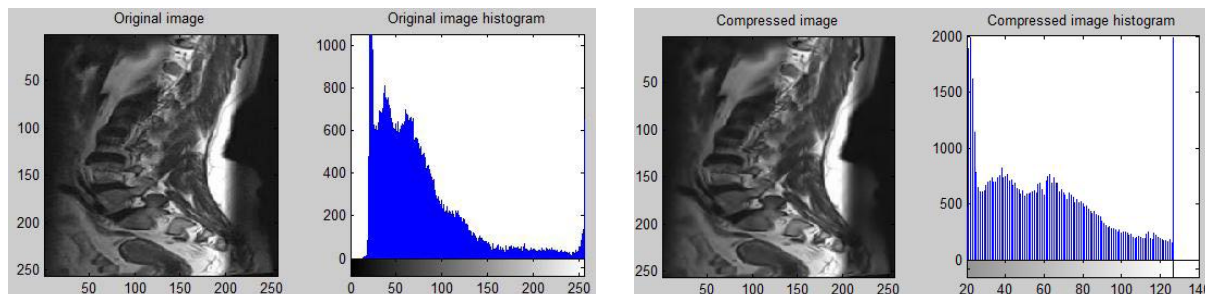
Figure 2: The structure of the wavelet transform based compression

6 The Results

6.1 Wavelet method results for CT-Scan medical image of brain (.jpg)



6.2 Wavelet method results for MRI medical image of Spine (.jpg)



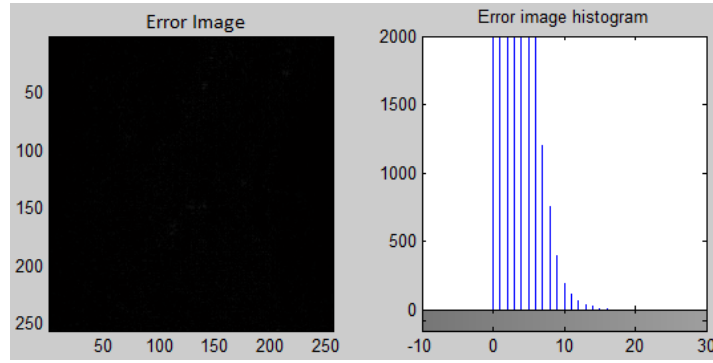

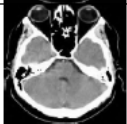
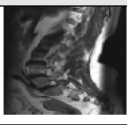
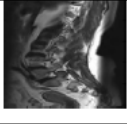
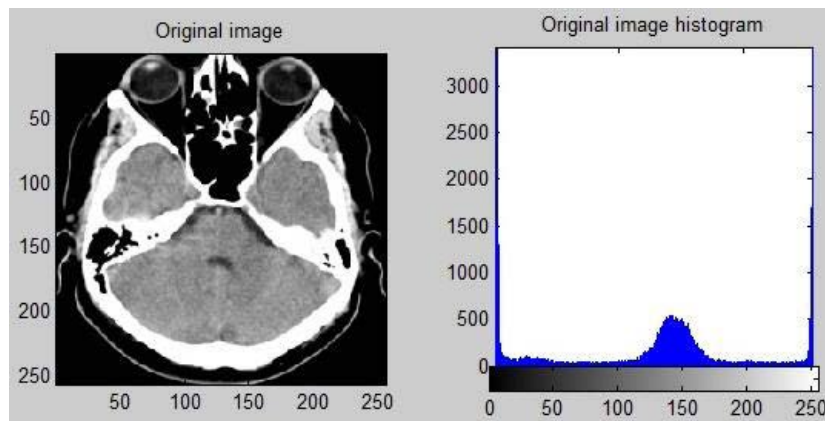


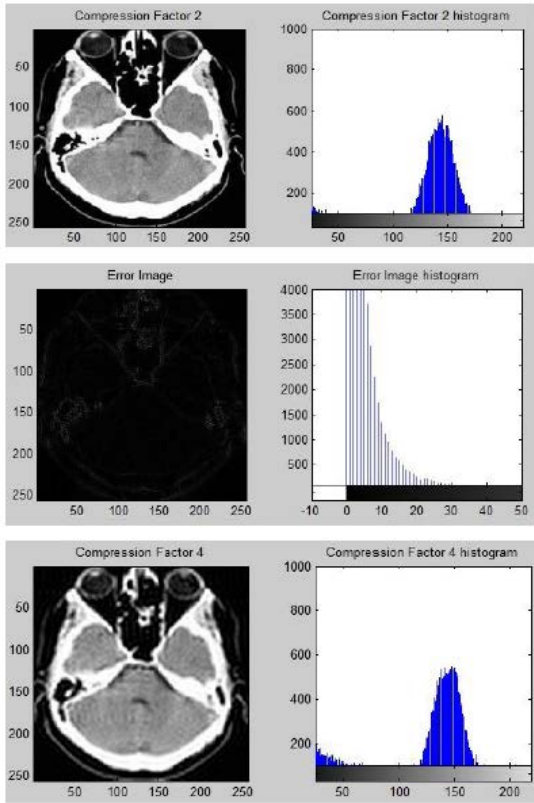
Table-1 results using Wavelet method for CT-Scan and MRI images

	Image type	Size(pixels) Resize image	Size(Kb) .jpeg	MSE	Psnr	Compression Ratio*	
1	CT -Origin medical(Brain. jpg)	256 x 256	12.9	-	-		
	Compressed Brain image	256 x 256	7.32	33.669	32.858	43.25	
2	MRI-Spine Origin	256 x 256	9.38				
	Spine- compressed	256 x 256	1.07	9.23	38.476	88.59	

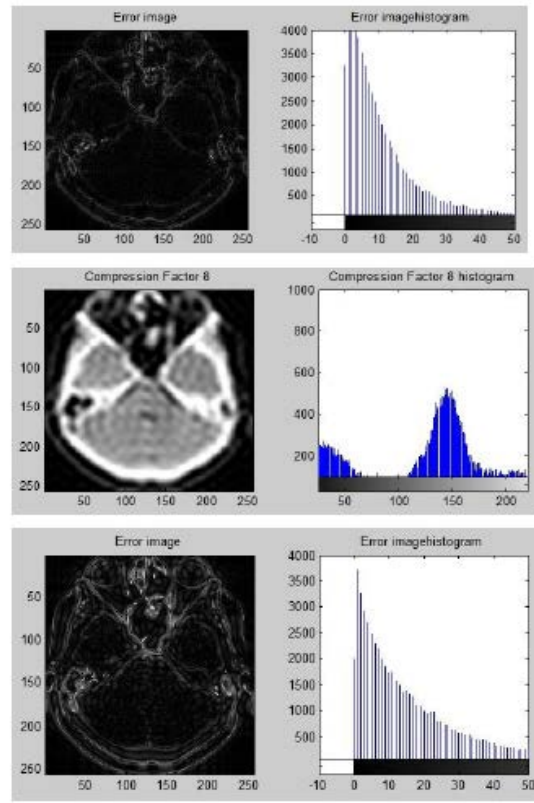
*CR = (original image size - compressed image size)/original image size*100%

6.3 Results using Discrete Cosine Transform (DCT) method for CT Brain image

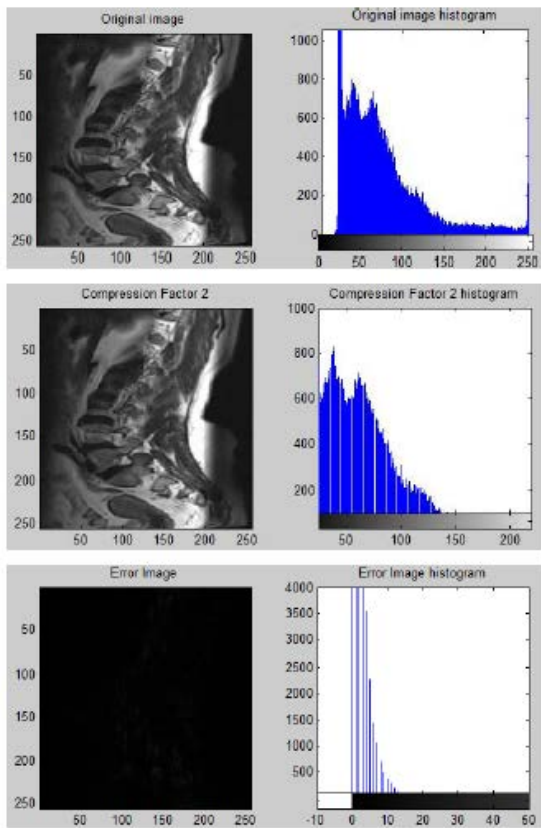




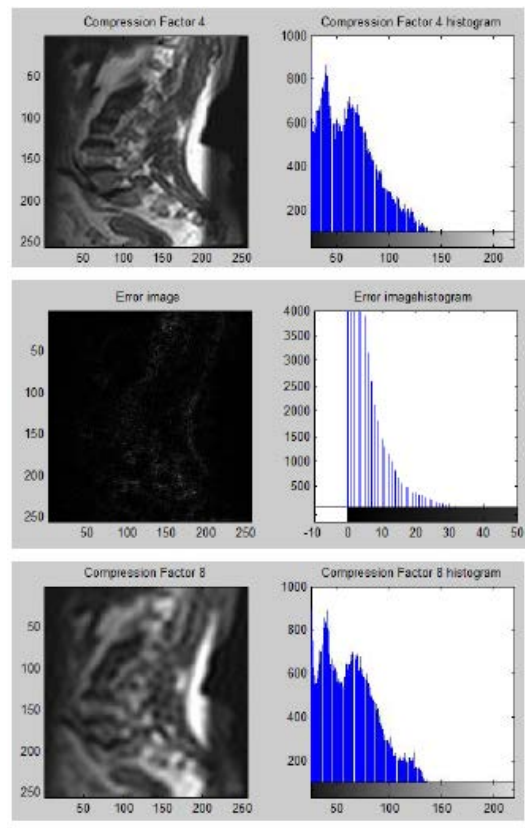
(a)



(b)



(c)



(d)

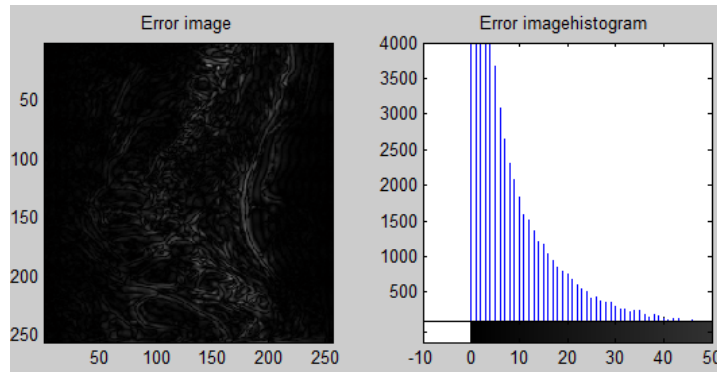




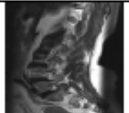

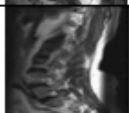
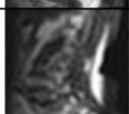


Table-2 results using DCT method for CT and MRI images

	Image type	Size(pixels)	Size(Kb) jpeg	MSE	Psnr	Compression Ratio*	
1	Origin medical-CT brain	256 x 256	12.9				
	Compression Factor 2	256 x 256	12.2	5.4649	40.755	5.4	
	Compression Factor 4	256 x 256	10.2	13.5615	36.8077	20.93	
	Compression Factor 8	256 x 256	7.77	23.5266	34.4152	39.76	
				MSE	Psnr		

2	Spine image origin	256 x 256	9.38	-	-	-	
	Spine- Compression Factor 2	256 x 256	9.05	2.0287	45.0586	3.5	
	Spine- Compression Factor 4	256 x 256	7.32	5.8727	40.4424	21.96	
	Spine- Compression Factor 8	256 x 256	5.46	9.9926	38.134	41.79	


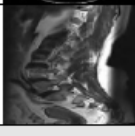

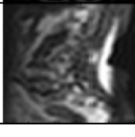
7 Conclusion

According to the results in the table below, the conclusions are:

- 1- Wavelet compression method for both CT and MRI images is better than DCT compression method.
- 2- In MRI images, the compression ratio is high using wavelet method, it is twice than the compression ratio of CT-Scan images.

- 3- The MSE and PSNR are approximately the same in both compression methods (wavelet and DCT) for MRI and CT scan images.
- 4- The quality of compressed images using wavelet is better than using DCT method and the error image is less than the error image using DCT method

Note: the size of all images used in this article is resize to 256 x 256 pixels

Image Type	Size(pixels)	Compression method	Compression ratio	MSE	PSNR	
CT	256 x 256	Wavelet	43.25	33.669	32.858	
		DCT	39.76	23.526	34.415	
MRI	256 x 256	Wavelet	88.59	9.23	38.476	
		DCT	41.79	9.99	38.134	

REFERENCES

- [1]. David Salomon A Concise Introduction to Data Compression. © Springer-Verlag London Limited 2008.
- [2]. Khalid Sayood Introduction to Data Compression.3rd edition. 2006 by Elsevier inc,
- [3]. Lossless and Transparency Encoding in WebP, https://developers.google.com/speed/webp/docs/webp_lossless_alpha_study?csw=1
- [4]. Prabhakar, Telagrapu, V .Jagan Naveen etal. Image compression using DCT and wavelet transformations, international journal of signal processing, image processing and pattern recognition , vol.4,No.3, September ,2011.
- [5]. Matlab the language of technical computing, version 7.6.0.324(R2008a), wcompress function.
- [6]. <http://eeweb.poly.edu/~onur/lectures/lecture2.pdf>. Onur G. Guleryuz, Department of Electrical and Computer Engineering, Polytechnic University, Brooklyn, NY 18
- [7]. David Salomon, Giovanni Motta, D. Bryant. Handbook of Data Compression, 5th edition. Springer-Verlag London Limited 2010.
- [8]. Rao K.R., Yip P.C. eds. The transform and data compression handbook 2001.CRC Press. Boca Raton London New York Washington, D.C

- [9]. Digital image processing using MATLAB by Rafael C. Gonzalez ,Richard E. Wood Steven L.Eddins,2004, Pearson Prentice Hall

- [10]. <http://www.cipr.rpi.edu/research/SPIHT/spiht1.html>

- [11]. M. Mozammel Hoque Chowdhury and Amina Khatun. Image Compression Using Discrete Wavelet Transform. IJCSI International Journal of Computer Science Issues, Vol. 9, Issue 4, No 1, July 2012

Saving of Etalons in Image Processing Systems Based on the Parallel Shift Technology

Stepan Bilan¹, Sergey Yuzhakov² and Sergii Bilan³

¹State Economy and Technology University of Transport, Kiev, Ukraine

²Haysin merged state tax inspection of Main governance of SFS in Vinnitsa region, Haysin, Ukraine

³Win-Interactive LLC, Vinnytsia, Ukraine

¹bstepan@ukr.net, ²yserg74@meta.ua, ³belan@svitonline.com

ABSTRACT

This article describes variants saving of etalons in image processing systems based on the parallel shift technology. The parallel shift technology can be used in hybrid image processing systems.

Keywords: parallel shift technology, function of the area of intersection, Fourier transformation.

1 Introduction

The use of hybrid systems to model any process is more productive than the use of systems that are based on a one method of information processing [1]. This article explains process description and saving of etalons in the systems which based on the use of multiple image transformations.

The digital image processing most widely used to manipulate with video information. This process is characterized by a description of the visual scene as a set of pixels. In this case, the formation of this set at digitization images are rather simple process. The main burden in image processing is to analyze a set of pixels [2]. The number of computational operations increases with discreteness digitized image.

It is proposed to describe visual scene also as a set of features for building a hybrid systems of image processing [3, 4]. The number of such functions must be significantly smaller than the number of digitized image pixels. That is, the set of pixels have to unite on certain features. The area of the specific image parts can be the unifying parameter. Its dynamic changes should be carried out to transform static area parameter to the function. The performance of certain image processing tasks is enhanced by reducing the computational operations that occurs as a result of reducing the number of objects for analysis.

Means of obtaining the function of the area of intersection (FAI) is a parallel shift technology (PST). PST is a process of interaction object that describes by n-dimensional characteristic features vector (CF), with a copy of which changes only one CF in comparison to the original. As a result, certain way got a superposition of the pair, which is different from the original object and can be used for further analysis. For example, the sum of the sinusoidal signal-copy which shifted in the phase space and its initial signal is different from a sinusoid. When phase shift is π , the sum will be zero. The change one of coordinates is using to obtain the function of the area of intersection. The result of the superposition of the original image and its parallel shifted copy is the FAI of these objects. A set of values of intersection area for each change of the coordinates is the FAI.

FAI is a function depending on intersection area of the original image and its copies which parallel shifted in the chosen direction, of the shift distance. The process of determining the area and parallel shift easily implemented using simple circuit solutions (Belan S. & Belan N., 2012).

FAI(x) is determined as the area of intersection of the image (Figure 1,a) and its copy, that is shifted in a parallel direction ϕ (Figure 1,b).

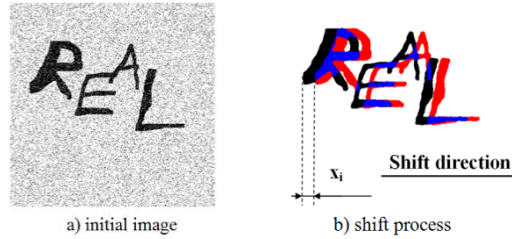


Figure 1: Image shift for FAI formation

Obtaining a pair of FAI by two orthogonal shifts (Figure 2).

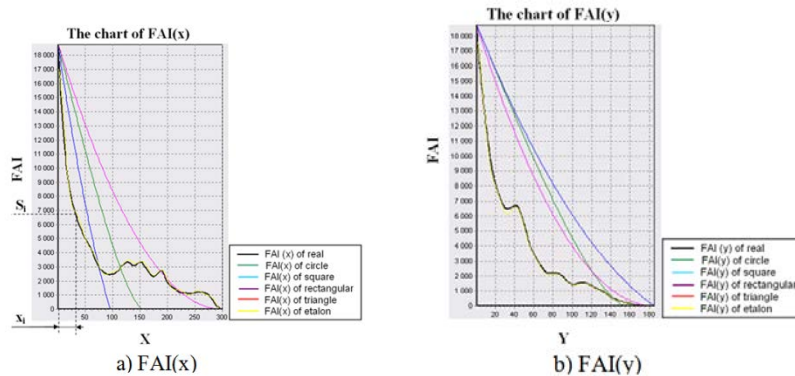


Figure 2: The functions of the area of intersection

In previous publications on this topic describes a variety of methods and algorithms for video processing using image transformation based parallel shift technology (Belan S. & Yuzhakov S., 2013). This article deals with the variants saving of etalon data.

2 Variants Saving of Etalon Data

One of the characteristics of image processing with PST is preservation etalons in the form of a certain etalon surfaces created by the function of the area of intersection in the direction of ϕ to $\phi + \pi$. Direction ϕ is the initial scan direction of image in the creation of etalon. It can be any direction. Only set of FAI reflects information about the shape of a particular object. Whatever kind of additional indicators were not used in the algorithms of image processing system to speed the processing steps, the final step is always the comparing real and etalon FAI.

The etalon surfaces may be stored as digitally and in analog form. Saving of etalon surfaces in digital form requires a large amount of hardware costs and requires additional processing facilities functions in comparison (requires scaling).

Variant of creating etalons for the reduction of the required information can be by saving of reduced etalon copies of images in the database. In this case, the values of etalon FAI can be generated from the reduced etalon directly in the detailed stage of recognition process. This method of saving will reduce the number of required hardware. But in this case it is increased the error in the recognition process. In addition, it does not eliminate the need for scaling functions.

Another method of etalons saving is to replace the etalons FAI by auxiliary functions which dependent on the input function of the area of intersection. At the stage of software simulation was used fast Fourier transformation (FFT). This version is simple in realization. It significantly reduce hardware costs and does not require additional processing methods of functions. Quantity of information required to store the etalon surface in the form of auxiliary function elements which depend on the number of etalons in the database.

Saving etalon surfaces in analog form can carry a highly accurate reflection of FAI. Using holography may be a variant of such saving. But the methods of processing such data description developed insufficiently. Image processing based on PST induces to development of new methods of information saving.

Procedure for the preparation of comparison etalon and real FAI in different variants of saving etalon surfaces is shown in Figure 3.

When using this method of describing images in analog computers is not compulsory digitization of FAI which obtained from the holography of etalon surfaces.

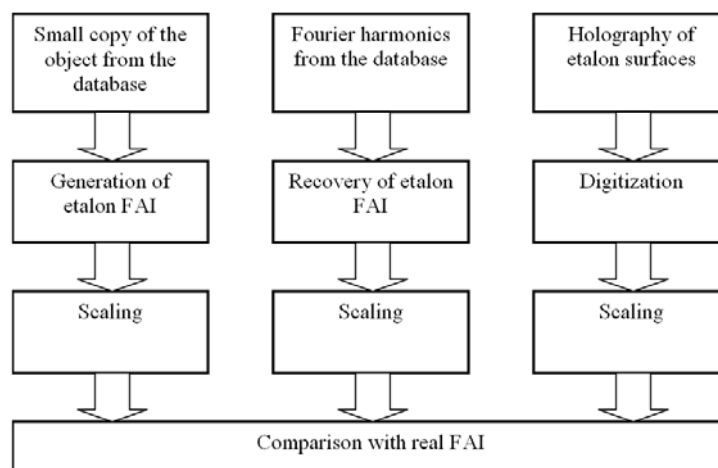


Figure 3: Procedure for the preparation of comparison etalon and real FAI in different variants of saving etalon surfaces

3 Transformation FAI to Fourier Series

A possible solution to the problem of etalon FAI saving is the use of Fourier transformation. As we know, such a transformation carries complete information about the function. The number of the Fourier series harmonics, which is necessary for saving the etalon surface, depending on the number of etalons. Normalization is required to unify the size values of harmonics. To achieve this, every element of series must be divided by the value of the input image area. In this case the value of all harmonics except the first are close to unity, which simplifies the storage of information in databases.

The following formulas for the normalized harmonics is used in constructing the Fourier series that reflect etalons FAI.

$$FFTN_0 = \frac{1}{S_0} \frac{1}{\sqrt{X_{\max}}} \sum_{j=0}^{X_{\max}-1} FAI(j), \tag{1}$$

$$FFTN_i = \frac{1}{S_0} \frac{\sqrt{2}}{\sqrt{X_{\max}}} \sum_{j=0}^{X_{\max}-1} FAI(j) \cdot \cos\left(\frac{\pi \cdot i \cdot (2 \cdot j + 1)}{2 \cdot X_{\max}}\right) \tag{2}$$

The value of the original image area (S_0) and maximal shift (X_{max}) are basic FAI parameters. Reverse recovery FAI occurs by the formula 3.

$$FAI(j) = S_0 \cdot \left(\frac{FFTN_0}{\sqrt{X_{max}}} + \frac{\sqrt{2}}{\sqrt{X_{max}}} \sum_{i=1}^{X_{max}-1} FFTN_i \cdot \cos\left(\frac{\pi \cdot i \cdot (2 \cdot j + 1)}{2 \cdot X_{max}}\right) \right), \tag{3}$$

The data set ($S_0, X_{max}, FFTN_0 \div FFTN_i$) taken from the etalon database.

Sample of saving etalon surface of the Chinese character "dragon" (Figure 4) by the first twenty harmonics of the Fourier series shown in Table 1.

Table 1: Example Description of Chinese Character "Dragon" in the Form of Normalized Values of the Fourier Series Harmonics in the Etalon Database

ID	WHAT	ANGLE	INTEGR	X_MAX	S_0	FFTN0	FFTN1	FFTN2	FFTN3	FFTN4	FFTN5	FFTN6	FFTN7	FFTN8	FFTN9	FFTN10	FFTN11	FFTN12	FFTN13	FFTN14	FFTN15	FFTN16	FFTN17	FFTN18	FFTN19	
1	dragon	0	0.2484	223	25077	3.7434	2.7350	0.3888	0.7211	0.7866	0.4466	0.3314	0.2356	0.1947	0.3951	0.2889	0.1578	0.1176	0.1259	0.0837	0.0572	0.0816	0.0657	0.0816	0.0657	0.0423
2	dragon	5	0.2403	211	25077	3.5249	2.5884	0.5322	0.7608	0.5743	0.4148	0.3246	0.2099	0.3579	0.3911	0.2111	0.1517	0.1228	0.1243	0.0549	0.0691	0.0895	0.0780	0.0500	0.0382	0.0382
3	dragon	10	0.2303	220	25077	3.4502	2.7628	0.5828	0.6247	0.6333	0.4252	0.3039	0.2553	0.3343	0.4126	0.2415	0.1304	0.1406	0.1173	0.0916	0.0572	0.0762	0.0899	0.0588	0.0441	0.0441
4	dragon	15	0.2296	228	25077	3.5002	2.7830	0.5509	0.6241	0.6984	0.4244	0.2970	0.2964	0.3109	0.4101	0.2852	0.1280	0.1349	0.1168	0.0773	0.0929	0.0864	0.0785	0.0630	0.0411	0.0411
5	dragon	20	0.2364	209	25077	3.4523	2.6366	0.5487	0.8016	0.5889	0.3759	0.3340	0.2947	0.4376	0.2998	0.1337	0.1387	0.1148	0.0966	0.0952	0.0924	0.0859	0.0515	0.0429	0.0307	0.0307
6	dragon	25	0.2281	217	25077	3.3940	2.4993	0.6216	0.9311	0.6195	0.3734	0.3415	0.3375	0.4066	0.3218	0.1707	0.1409	0.1172	0.1115	0.0942	0.0892	0.0800	0.0594	0.0392	0.0320	0.0320
7	dragon	30	0.2397	207	25077	3.4836	2.3288	0.5683	1.0049	0.5860	0.3950	0.3128	0.4539	0.3814	0.2369	0.1609	0.1339	0.1195	0.0930	0.0958	0.0751	0.0599	0.0425	0.0369	0.0299	0.0299
8	dragon	35	0.2234	223	25077	3.3893	2.4404	0.6595	0.8800	0.5517	0.4929	0.3849	0.4042	0.4234	0.2717	0.2055	0.1778	0.1319	0.1028	0.0990	0.0824	0.0618	0.0588	0.0386	0.0427	0.0427
9	dragon	40	0.2139	238	25077	3.3322	2.5023	0.7118	0.8625	0.5131	0.3756	0.4308	0.5429	0.4317	0.2534	0.2397	0.2238	0.1672	0.1317	0.0905	0.0888	0.0716	0.0565	0.0517	0.0464	0.0464
10	dragon	45	0.2113	244	25077	3.3328	2.5884	0.7595	0.7620	0.4950	0.3417	0.4160	0.5636	0.4319	0.3110	0.2326	0.2210	0.2009	0.1533	0.1123	0.0889	0.0543	0.0586	0.0585	0.0453	0.0453
11	dragon	50	0.2095	251	25077	3.3502	2.5929	0.7748	0.8144	0.4287	0.3149	0.4816	0.5107	0.3367	0.3110	0.3054	0.2598	0.2183	0.1749	0.1220	0.1034	0.0709	0.0521	0.0585	0.0585	0.0489
12	dragon	55	0.2130	254	25077	3.4266	2.5845	0.7840	0.8178	0.3733	0.4440	0.4659	0.3687	0.3816	0.2275	0.2604	0.3351	0.2527	0.1951	0.1290	0.1040	0.0791	0.0717	0.0594	0.0489	0.0489
13	dragon	60	0.2159	250	25077	3.4457	2.6092	0.8201	0.7174	0.4606	0.5349	0.3472	0.3303	0.2655	0.2726	0.2304	0.2835	0.2843	0.2197	0.1489	0.1098	0.0637	0.0696	0.0544	0.0544	0.0544
14	dragon	65	0.2083	258	25077	3.3451	2.7951	0.8653	0.6833	0.5937	0.4954	0.2780	0.2379	0.2623	0.2386	0.2215	0.2159	0.2436	0.2774	0.2161	0.1559	0.1083	0.0727	0.0469	0.0552	0.0552
15	dragon	70	0.2219	248	25077	3.5127	2.7654	0.8722	0.8025	0.4923	0.3099	0.2732	0.2459	0.2095	0.2544	0.2004	0.2314	0.2184	0.2420	0.2156	0.1686	0.0916	0.0557	0.0525	0.0487	0.0487
16	dragon	75	0.2237	254	25077	3.5970	2.9239	0.9578	0.7234	0.3631	0.3011	0.2774	0.2122	0.1761	0.2351	0.2225	0.2223	0.1933	0.1771	0.2012	0.2408	0.1703	0.0882	0.0463	0.0418	0.0418
17	dragon	80	0.2523	234	25077	3.8076	3.0107	0.8980	0.5797	0.3288	0.2885	0.2268	0.1895	0.2252	0.2602	0.2102	0.1829	0.1892	0.1891	0.2471	0.2011	0.0891	0.0482	0.0429	0.0591	0.0591
18	dragon	85	0.2744	240	25077	4.2035	3.0589	0.4227	0.6095	0.2417	0.2573	0.2463	0.1717	0.2008	0.2607	0.2085	0.1852	0.1788	0.1525	0.2017	0.2409	0.1851	0.0895	0.0432	0.0551	0.0551
19	dragon	90	0.2853	239	25077	4.4426	3.0347	0.3870	0.5370	0.3300	0.3187	0.2340	0.2038	0.1952	0.2621	0.1616	0.1878	0.1764	0.1371	0.1927	0.2192	0.1717	0.1105	0.0728	0.0542	0.0542
20	dragon	95	0.2959	258	25077	4.1569	3.0818	0.6091	0.5263	0.3016	0.3530	0.2448	0.2341	0.1543	0.2514	0.2132	0.1311	0.1889	0.1843	0.2009	0.1661	0.2005	0.1799	0.1403	0.0837	0.0837
21	dragon	100	0.2436	261	25077	3.9660	2.9892	0.6520	0.6396	0.3458	0.3456	0.3158	0.2704	0.2035	0.2648	0.2133	0.1266	0.1745	0.2105	0.2725	0.1341	0.1732	0.1860	0.1672	0.1015	0.1015
22	dragon	105	0.2378	256	25077	3.8365	2.8732	0.6012	0.7046	0.4469	0.3329	0.3004	0.2561	0.2173	0.2312	0.2016	0.1555	0.2154	0.1882	0.2609	0.1449	0.1470	0.1892	0.1612	0.0916	0.0916
23	dragon	110	0.2293	261	25077	3.7360	2.7801	0.6963	0.6821	0.4509	0.4035	0.3053	0.3260	0.2070	0.2259	0.1805	0.1785	0.2339	0.1971	0.2127	0.1363	0.1416	0.1832	0.1765	0.1088	0.1088
24	dragon	115	0.2162	272	25077	3.5957	2.7480	0.7898	0.6588	0.4059	0.4363	0.4013	0.3223	0.2544	0.2486	0.1615	0.1858	0.2386	0.2338	0.1417	0.1228	0.1158	0.1705	0.1767	0.1407	0.1407
25	dragon	120	0.2031	286	25077	3.4646	2.7711	0.8298	0.6880	0.4275	0.3759	0.4411	0.3498	0.2989	0.3005	0.1875	0.1676	0.2071	0.2737	0.1516	0.1321	0.1258	0.1500	0.1597	0.1583	0.1583
26	dragon	125	0.1946	299	25077	3.3933	2.7538	0.8748	0.6833	0.4961	0.3881	0.3185	0.3540	0.3688	0.3840	0.2610	0.1500	0.1918	0.2980	0.1636	0.1474	0.1232	0.1337	0.1587	0.1742	0.1742
27	dragon	130	0.1861	311	25077	3.3095	2.7131	0.9151	0.6854	0.4781	0.4531	0.2697	0.2657	0.3812	0.4510	0.3408	0.1688	0.2386	0.2629	0.1829	0.1466	0.1073	0.1409	0.1678	0.1732	0.1732
28	dragon	135	0.1993	286	25077	3.3999	2.5983	0.7839	0.6579	0.4877	0.4479	0.2232	0.2473	0.4654	0.4086	0.2872	0.3081	0.2410	0.1521	0.1196	0.1466	0.1791	0.1881	0.1369	0.1110	0.1110
29	dragon	140	0.1905	292	25077	3.2839	2.6795	0.7860	0.5759	0.4959	0.5244	0.3006	0.2839	0.3593	0.4365	0.4298	0.3160	0.2316	0.1469	0.1447	0.1609	0.1894	0.1616	0.1163	0.1082	0.1082
30	dragon	145	0.1999	274	25077	3.3398	2.5920	0.6960	0.5335	0.5314	0.5586	0.2808	0.3087	0.3688	0.4735	0.4185	0.3382	0.1763	0.1973	0.1992	0.1701	0.1201	0.1135	0.0847	0.0797	0.0797
31	dragon	150	0.2084	269	25077	3.3179	2.5799	0.6767	0.5031	0.6510	0.5067	0.2937	0.3738	0.2935	0.4589	0.3589	0.2823	0.2337	0.2286	0.1542	0.1284	0.1159	0.0805	0.0736	0.0920	0.0920
32	dragon	155	0.1851	289	25077	3.1758	2.7355	0.7241	0.4505	0.6636	0.5798	0.3902	0.3071	0.2846	0.3419	0.2892	0.3976	0.3806	0.2365	0.1509	0.1411	0.1279	0.0854	0.0708	0.0892	0.0892
33	dragon	160	0.1943	272	25077	3.2344	2.7315	0.6010	0.5011	0.7024	0.5885	0.3832	0.2671	0.2806	0.2921	0.4063	0.4403	0.2559	0.1688	0.1390	0.1095	0.0850	0.0906	0.0880	0.0816	0.0816
34	dragon	165	0.2023	240	25077	3.4456	2.5331	0.4565	0.6753	0.6771	0.5303	0.2768	0.3060	0.3574	0.3726	0.3840	0.2677	0.1489	0.1041	0.1070	0.1137	0.0957	0.0634	0.0711	0.0878	0.0878
35	dragon	170	0.2276	230	25077	3.4842	2.5326	0.4477	0.6563	0.6972	0.4887	0.3528	0.3222	0.2160	0.3844	0.3957	0.2056	0.1029	0.1145	0.1318	0.0931	0.0637	0.0775	0.0875	0.0721	0.0721
36	dragon	175	0.2347	228	25077	3.5766	2.5877	0.3909	0.6495	0.7297	0.5390	0.3550	0.2742	0.1953	0.3986	0.3710	0.1740	0.1169	0.1465	0.1079	0.0762	0.0738	0.0804	0.0857	0.0637	0.0637



Figure 4: Image of Chinese character "dragon"

We can use for the reverse transformation not all Fourier series, but only a part of it, for a certain approximation to the shape of the input function. It is similar to the process of low-frequency filtration. The software simulation revealed that for the creation etalon FAI of convex shapes rather

use the first five Fourier harmonics. For the creation etalon FAI of not convex shapes rather use the first ten Fourier harmonics. To create the etalon FAI of images which consist of several objects enough to use the first twenty Fourier harmonics. In all these cases the deviation of the restored FAI and real FAI does not exceed 10% of the real value of the function at each step shift. Also, when comparing the functions, you can use mean square deviation the real FAI and etalon FAI for a specific functions plot.

We can simulate the forgetting process with saving of etalon functions as Fourier series. Suppose that after the learning process the FAI described by the full set of the Fourier series harmonics. The number of elements of the series will coincide with the length of digitized function. The harmonic with the largest number can be removed from the etalon at regular intervals. Some information about the etalon to be lost, but will decrease the data which required to saving. Repeated recovery of the object becomes necessary when a function is based on the current number of harmonics will differ from the original by more than a specified value. Formula 3 turns to the next when the selected number of harmonics of the Fourier series (NH) to restore the FAI.

$$FAI(j) = S_0 \cdot \left(\frac{FFTN_0}{\sqrt{X_{\max}}} + \frac{\sqrt{2}}{\sqrt{X_{\max}}} \sum_{i=1}^{NH-1} FFTN_i \cdot \cos\left(\frac{\pi \cdot i \cdot (2 \cdot j + 1)}{2 \cdot X_{\max}}\right) \right), \quad (4)$$

For example, for the image from the Figure 4 the FAI charts when using a certain number of the first Fourier series harmonic are as follows (Figure 5).

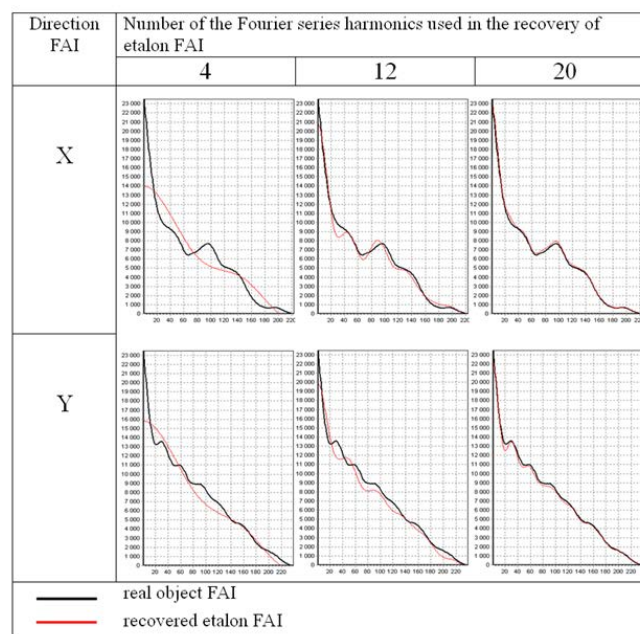


Figure 5: The charts of real object FAI and recovered etalon FAI

4 Conclusion

Saving of etalon information as functions can significantly reduce the amount of storage data. Image processing using the function of the area of intersection will speed the recognition process, the definition of spatial orientation and the movement parameters of the 2D-objects. However, the images recovery process with help of etalon surface is very complex.

The principles of manipulation with the 2D-objects can be used for the analysis of higher dimension objects. In this case, we must have the detectors intersection of objects with their copies.

The objects of image processing research based parallel shift technology were the 2D binary image. Future plans to conduct research of processing grayscale images and scene analysis.

REFERENCES

- [1]. Castillo O., Mellin P. *Hybrid Intelligent Systems*, Heidelberg (Germany): Springer, 2006.
- [2]. Gonzalez R.C., Woods R. E., Eddins S. L. *Digital Image Processing using MATLAB*. Pearson Prentice-Hall, 2004.
- [3]. Belan S., Yuzhakov S., *A Homogenous Parameter Set for Image Recognition Based on Area*, Computer and Information Science, 2013. 6(2): p. 93-102.
- [4]. Belan S., Yuzhakov S., *Machine Vision System Based on the Parallel Shift Technology and Multiple Image Analysis*, Computer and Information Science, 2013. 6(4): p. 115-124.